Cognitive Neurodynamics (2023) 17:1093–1113
https://doi.org/10.1007/s11571-022-09872-5

RESEARCH ARTICLE

Nonlinear mechanism for the enhanced bursting activities induced by fast inhibitory autapse and reduced activities by fast excitatory autapse

Changsheng Qi[1] · Yuye Li[2] · Huaguang Gu[3] · Yongxia Yang[2]

Received: 28 December 2021 / Revised: 28 July 2022 / Accepted: 13 August 2022 / Published online: 21 August 2022

Abstract

The paradoxical phenomena that excitatory modulation does not enhance but reduces or inhibitory modulation not suppresses but promotes neural firing activities have attracted increasing attention. In the present study, paradoxical phenomena induced by both fast excitatory and inhibitory autapses in a "Fold/Big Homoclinic" bursting are simulated, and the corresponding nonlinear and biophysical mechanisms are presented. Firstly, the enhanced conductance of excitatory autapse induces the number of spikes per burst and firing rate reduced, while the enhanced inhibitory autapse cause both indicators increased. Secondly, with fast-slow variable dissection, the burst of bursting is identified to locate between a fold bifurcation and a big saddle-homoclinic orbit bifurcation of the fast subsystem. Enhanced excitatory or inhibitory autapses cannot induce changes of both bifurcation points, i.e., burst width. However, width of slow variable between two successive spikes within a burst becomes wider for the excitatory autapse and narrower for the inhibitory autapse, resulting in the less and more spikes per burst, respectively. Last, the autaptic current of fast autapse mainly plays a role during the peak of action potential, differing from the slow autaptic current with exponential decay, which can play roles following the peak of action potential. The fast excitatory autaptic current enhances the amplitude of the action potential and reduces the repolarization of the action potential to lengthen the interspike interval (ISI) of the spiking of the fast subsystem, resulting in the wide width of slow variable between successive spikes. The fast inhibitory autaptic current reduces the amplitude of action potential and ISI of spiking, resulting in narrow width of slow variable. The novel example of the paradoxical responses for both fast modulations and nonlinear mechanism extend the contents of neurodynamics, which presents potential functions of the fast autapse.

Keywords Bifurcation · Excitatory autapse · Inhibitory autapse · Bursting

Introduction

The nervous system processes information through complex nonlinear electrical activities, which are involving in sensory, cognitive, and motor control functions (Glass 2001; Ma et al. 2021; Yang et al. 2018; Mondal et al. 2019). Bursting behavior is one of the most important electrical activities, which is suggested as the basic unit of information processing (Lisman 1997). The transitions or bifurcations of bursting modulated by different factors such as temperature, blood, and ion concentration are related to the information encoding (Braun et al. 1994; Gu and Pan 2015; Duan et al. 2020). In addition, different bursting patterns have been found in different neurons (Izhikevich 2000; Duan et al. 2021; Liu and Liu 2020; Liu et al. 2020) or in different states of a same neuron. For example, bursting in the lateral habenula neuron is related to depression (Yang et al. 2018) and in the stomatogastric ganglion (STG) to digestive function (Cazalets et al. 1987). In appearance, bursting alternates between a burst

✉ Yuye Li
liyuye2000@163.com

[1] College of Chemistry and Life Sciences, Chifeng University, Chifeng 024000, China

[2] College of Mathematics and Computer Science, Chifeng University, Chifeng 024000, China

[3] School of Aerospace Engineering and Applied Mechanics, Tongji University, Shanghai 200092, China

containing multiple spikes and a long quiescent state. In theory, bursting often appears in the nonlinear system containing fast variables and a slow variable (Negro et al. 1998; Izhikevich et al. 2003; Gu and Pan 2015). When the slow variable is regarded as a control parameter, the fast subsystem (fast variables) often exhibits the coexistence of stable equilibrium point and limit cycle related to bifurcations, which can be used to characterize the dynamics of the bursting. For example, for the "Fold/Homoclinic" bursting pattern, the burst begins and terminates respectively via fold and saddle-homoclinic orbit bifurcation, respectively. Many bursting patterns are identified according to different bifurcations. In the real nervous system, the neurons with bursting patterns receive inhibitory and/or excitatory currents through synapses (Bacci and Huguenard 2006; Yin et al. 2018; Kim and Lim 2020). In general, excitatory and inhibitory modulations respectively promote and inhibit the neuronal electrical activities (Goldwyn et al. 2018; Gu et al. 2021; Vida et al. 2006). Under the regulation of inhibitory or excitatory synapses, the electrical activities of nervous system achieve dynamic balance to ensure the stability of physiological function.

Except for the various electrical activities consistent with the general viewpoint, there are many investigations on the paradoxical electrical responses opposite to the general viewpoint (Satterlie 1985; Beiderbeck et al. 2018; Li et al. 2019; Wu and Gu 2020; Cao et al. 2021; Wang et al. 2020), which enrich the contents of neurodynamics. For example, an inhibitory stimulus instead of excitatory stimulus induces a spike from the resting state, i.e., a post-inhibitory rebound (PIR) spike, which is prevalent in many nervous systems and plays important roles in the information processing and motor control (Satterlie 1985; Zhao et al. 2018). In addition, an inhibitory stimulus applied prior to an excitatory effect can lead to the enhancement of electrical activities, which is called post-inhibitory facilitation (PIF) and plays important roles in the spatial localization of auditory nervous system (Beiderbeck et al. 2018; Dodla and Rinzel 2006). As the firing frequency of the inhibitory neuron increases, the stimulation of the inhibitory neuron to pyramidal neuron becomes strong. However, the behavior of the pyramidal neuron changes from tonic firing to depolarization block corresponding to spread depression, which may be related to migraine (Auffenberg et al. 2021; Chever et al. 2021). In addition, anticipated synchronization is another interesting paradoxical phenomenon, which is observed in a system composed of a sender neuron with unidirectional excitatory synapse to a receiver neuron stimulated by an inhibitory neuron (Matias et al. 2011). In common viewpoint, the response of the receiver neuron appears after the stimulation of the sender neuron, which corresponds to delay synchronization. However, the response of the receiver neuron appears before the stimulation of the sender neuron, which corresponds to the anticipated synchronization. Recently, the anticipated synchronization is simulated population neurons and observed in electroencephalogram in different brain regions (Matias et al. 2015; Carlos et al. 2020). In the theoretical models, it has been found that the excitatory effects can impede the generation of spikes (Wu and Gu 2020; Cao et al. 2018) and inhibitory effects can promote the generation of spikes (Dodla and Rinzel 2006; Dodla et al. 2006) in single neurons, excitatory synapse induces the disappearance of the firing activity (Uzuntarla et al. 2019) and inhibitory synapse promotes the synchronization or firing rate of the neuronal networks (Elson et al. 2002; Jia et al. 2018). These results suggest that paradoxical phenomena and their regulatory mechanisms are important to understand the complex dynamical behaviors of the nervous system.

Recently, autapse (a synapse beginning and terminating at a same neuron) in various neurons (hippocampus (Cobb et al. 1997), neocortex (Bacci and Huguenard 2006), and visual cortex (Tamás et al. 1997)) has received a lot of attention. The excitatory autapse is identified to evoke persistent firing (Saada et al. 2009) or promote bursting activity (Yin et al. 2018). The inhibitory autapse inhibits the action potential (Bacci et al. 2003). On the contrary, the inhibitory self-feedback can induce PIR spike (Tikidji-Hamburyan et al. 2015). In networks, inhibitory autapse induce Gamma synchronization (Deleuze et al. 2019). Except for the above experimental results, firing activities of single neurons (Wang et al. 2014; Guo et al. 2016; Song et al. 2019; Xu et al. 2017; Zhao and Gu 2017) and spatiotemporal dynamics of networks (Ge et al. 2018; Ma et al. 2015; Yang et al. 2017; Wang et al. 2011; Yilmaz and Ozer 2015; Uzun et al. 2017; Yilmaz et al. 2016; Ge et al. 2019) induced by autapse have been studied in theoretical models such as the Hodgkin–Huxley (HH) model, Morris-Lecar (ML) model, Hindmarsh–Rose (HR) model, FitzHugh–Nagumo (FHN) model, Wang–Buzsaki (WB) model, which contain the complex and paradoxical phenomena. For example, autapse can induce the bifurcation and chaos in the HR model (Xu et al. 2017) and the transition between class I and II excitabilities in the ML model (Zhao and Gu 2017). In addition, inhibitory autapse can induce PIR spiking in the HH model when time delay is suitable (Zhao et al. 2020a), which presents theoretical explanation to the experimental observation in the Ref. Tikidji-Hamburyan et al. (2015). Recently, the enhanced coherence resonance of single neurons or networks with spiking behaviors induced by inhibitory autapse (Ding et al. 2021; Jia et al. 2021; Yao et al. 2019) or by electrical autapse (Yilmaz et al. 2016; Baysal et al. 2021) is identified. Excitatory autapse suppresses neural spiking activity near subcritical Hopf bifurcation when time delay is

propriate in the Hodgkin–Huxley (HH) model (Zhao et al. 2020b).

Except for the spiking activity, paradoxical phenomena for different bursting patterns induced by autapses have attract much attention. On one hand, time delay is considered in many studies on the autapse (Cao et al. 2021, 2018; Ding and Li 2016). For the "Fold/Homoclinic" bursting, inhibitory autapse promotes firing frequency (Ding and Li 2016), and excitatory autapse can induce less spikes per burst but higher firing frequency in the Rulkov model (Cao et al. 2018). For other two bursting patterns ("Homoclinic/Homoclinic" bursting in the modified FHN model (Hua et al. 2020) and "Circle/Fold cycle" bursting in the modified ML model (Cao et al. 2021)), the excitatory autapse can induce less spikes and lower firing rate. However, for "Fold/Big Homoclinic" bursting in the modified FHN model, excitatory modulation can induce less spikes per burst for suitable time delay and strength of autapse (Cao et al. 2021). On the other hand, time delay is not considered for the autapse (Li et al. 2019; Wang et al. 2020; Chay 1985; Li et al. 2021; Lu et al. 2021). For the "Fold/Homoclinic" bursting, the responses to the autapses exhibit model-dependent. In the Chay model (Chay 1985), inhibitory autapse can induce paradoxical phenomenon (Li et al. 2019, 2021), while the excitatory autapse just induce the common response (Li et al. 2021). However, in the modified ML model, inhibitory autapse can induce paradoxical phenomenon (Lu et al. 2021) and excitatory autapse can suppress the bursting activity (Wang et al. 2020).

More importantly, with help of bifurcations of the fast subsystem, the dynamical mechanisms for the paradoxical phenomena of bursting patterns are acquired. For the condition of autapse with time delay (Cao et al. 2021, 2018; Ding and Li 2016), the autaptic current is not contained in the fast subsystem, and the autaptic current pulse is regarded as a disturbance, which plays a role at a phase determined by the time delay. When the phase is near the boundary between the attraction domains of coexisting behaviors and the pulse is strong enough (determined by the autaptic conductance) to induce the phase trajectory of bursting run across the boundary, paradoxical phenomenon is induced. For the case of autapse without time delay (Li et al. 2019; Wang et al. 2020; Li et al. 2021; Lu et al. 2021), the fast subsystem contains the autaptic current. The bifurcation points or bifurcation types of the fast subsystem change with respect to the change of the autaptic conductance, resulting in the changes of burst duration or spike number per burst (Li et al. 2019; Wang et al. 2020; Li et al. 2021; Lu et al. 2021), i.e., the paradoxical phenomenon. All these indicate that fast-slow variable dissection method can be effectively used to identify the underlying dynamics of the paradoxical phenomena of bursting behaviors. In addition, the different roles of ionic or autaptic currents in modulating the dynamics or bifurcations of the fast subsystem are acquired (Wang et al. 2020; Li et al. 2021), which is the biophysical mechanism for the paradoxical phenomena. Up to now, complex and various dynamics and mechanisms of the paradoxical phenomena have been acquired for only several bursting patterns, which exhibit dependence to the bursting patterns or theoretical models (Li et al. 2019; Cao et al. 2021; Wang et al. 2020; Cao et al. 2018; Ding and Li 2016; Li et al. 2021; Lu et al. 2021). Considering that there exist many different bursting patterns in the real nervous system, to present comprehensive viewpoints of the paradoxical phenomena of bursting patterns induced by autapses is important for the neurodynamics and nonlinear physics such as the paradoxical phenomena, the potential functions of the autapse, and the measures to modulate the brain neurons.

In the present study, we present a novel example and mechanism of paradoxical phenomenon induced by excitatory autapse and inhibitory autapse respectively in the "Fold/Big Homoclinic" bursting pattern. Different from the previous study (Cao et al. 2021), inhibitory autapse and no time delay are considered in the present study. And different from the previous study (Li et al. 2019; Wang et al. 2020; Li et al. 2021; Lu et al. 2021), excitatory and inhibitory autapses induce the paradoxical responses in a same model. Firstly, excitatory or inhibitory self-feedbacks/autapses induce paradoxical responses. For the excitatory autapse, less spikes per burst and lower firing rate are induced. For the inhibitory autapse, the spike number per burst increases and the firing rate enhances. Secondly, the dynamical mechanisms of the paradoxical responses are acquired with the bifurcations of the fast subsystem. Different from the results of previous investigations wherein the bifurcation types or points change with respect to the autaptic conductance (i.e., the burst width changes) (Li et al. 2019; Cao et al. 2021; Wang et al. 2020; Ding and Li 2016; Li et al. 2021; Lu et al. 2021), the bifurcation points remain nearly unchanged in the present paper. However, the interval between spikes within burst changes with respect to the autaptic conductance, resulting in the change of spike number per burst. The spike number per burst decreases and increases for the excitatory and inhibitory autapses, respectively, which are the cause for the paradoxical phenomena. Last, the roles of the autaptic current in modulating the interval between the spikes are identified. The results present a novel example that excitatory and inhibitory autapses respectively induce paradoxical responses of an identical bursting pattern and novel dynamical mechanisms for the paradoxical phenomena, which enrich the contents of neurodynamics, provide

practical feedback measures to modulate neuronal bursting activities, and present potential functions of the autapse.

The rest of the present paper are organized as follows. Sections "Theoretical model and methods", "Results", and "Conclusion and discussion" present model and method, results, and conclusion, respectively.

Theoretical model and methods

Modified FitzHugh–Nagumo model

Considering the autapse, the modified FitzHugh–Nagumo (FHN) model (Izhikevich 2000; Cao et al. 2021) is described as follows:

$$\frac{dV}{dt} = V - \frac{V^3}{3} - \omega, \tag{1}$$

$$\frac{d\omega}{dt} = \varepsilon(-u + V - S(\omega)), \tag{2}$$

$$\frac{du}{dt} = \mu(u_p + V). \tag{3}$$

where V is the membrane potential, ω is the recovery variable, and u is a slow variable to modulate the bursting activity via the regulation to ω (Eq. 2). The parameter μ and u_p are used to control the values of the slow variable u. The parameter μ is a feedback coefficient, and u_p plays a role like the "reversal potential". The expression of function $S(\omega)$ is given by:

$$S(\omega) = b/\left(1 + e^{\frac{c-\omega}{d}}\right) \tag{4}$$

In the present paper, the effect of autapse on "Fold/Big Homoclinic" bursting is studied in the modified FHN model. To simulate the "Fold/Big Homoclinic" bursting, except for the parameter u_p, other parameter values are chosen from the Refs. Izhikevich (2000) and Cao et al. (2021) and shown as follows: $\varepsilon = 0.15$, $\mu = -0.0005$, $b = 1.75$, $c = -0.5$, and $d = 0.1$. The u_p is chosen as control parameter to modulate the bursting patterns.

Synapse model

There are multiple theoretical models to describe the dynamics of synapse, among which a fast threshold modulatory synapse model (Wang and Rinzel 1992) and α-dynamical synapse model with exponential decay characteristic (Wang and Buzsöki 1996; Van Vreeswijk et al. 1994) are widely studied. The fast threshold modulatory synapse is described by the Boltzmann function, which is given by:

$$I^{syn} = -g^S(V_{post}(t) - V^S)\Gamma(V_{pre}(t)) \tag{5}$$

where I^{syn} is the synapse current, g^S represents the conductance of synapse, $V_{post}(t)$ is the membrane potential of the postsynaptic neuron, V^S is the reversal potential of synapse, and $V_{pre}(t)$ is membrane of presynaptic neuron (Zhao et al. 2020b).

$$\Gamma(V_{pre}(t)) = 1/(1 + e^{-\lambda(V_{pre}(t)-\theta_S)}) \tag{6}$$

where θ_S is the threshold of synapse current, which mainly determines the pulse duration. The parameter λ means the release rate of the transmitter, which determines the changing speed of the pulse current. Fast threshold modulatory synapse is a remarkable model of a realistic fast synapse (Rubin and Terman 2000), such as that in the leech heart center pattern generator (Cymbalyuk et al. 2002), as it yields a nearly instantaneous response from the synapse on the postsynaptic neuron. The synaptic current of fast threshold modulatory autapse does not exhibit exponential decay following a spike.

However, many physiological synapses have a slower rate of neurotransmitter dynamics than that of the channels, generally referred to as the slow synapses (Debanne et al. 2011). The slow synaptic current of slow synapse exhibit exponential decay following a spike, which is described by the ordinary differential equation, for example, the α-dynamical synapse with exponential decay (Wang and Buzsöki 1996; Van Vreeswijk et al. 1994), which is given by:

$$I^{syn} = -g^S(V_{post}(t) - V^S)s \tag{7}$$

$$\frac{ds}{dt} = \alpha_S(1 - s)\Gamma(V_{pre}(t)) - \beta_S s \tag{8}$$

$$\Gamma(V_{pre}(t)) = 1/(1 + e^{-\lambda(V_{pre}(t)-\theta_S)}) \tag{9}$$

where I^{syn} is the synapse current, g^S represents the conductance of synapse, $V_{post}(t)$ is the membrane potential of the postsynaptic neuron, V^S is the reversal potential of synapse, and $V_{pre}(t)$ is membrane of presynaptic neuron. The variable s is the gating variable. α_S and β_S denote the rise and decay constants of the autaptic current, respectively. The rise constant α_S determines the rising speed of the autaptic current. The larger the value α_S is, the faster the autaptic current rises. The decay constant β_S determines the decay speed of the autaptic current. The smaller the value β_S is, the slower the autaptic current decays. For a relatively small β_S, the autaptic current exhibits exponential decay following a spike. $\Gamma(V_{pre}(t)) = 1/(1 + e^{-\lambda(V_{pre}(t)-\theta_S)})$ is an active function, where the parameter θ_S is the half-activation value, and λ is the activation rate.

For an autapse model, $V_{post}(t) = V_{pre}(t) = V(t)$. In the previous studies, fast autapse and slow autapse have different effects on the depolarization block near a Hopf

bifurcation. Slow autapse can induce firing from depolarization bock (Zhao et al. 2016) and fast autapse induce subthreshold oscillations (Jia 2018). In the present paper, the autaptic current of fast threshold modulatory autapse is studied.

Modified FitzHugh–Nagumo model with autapse

Because the fast threshold modulatory autapse is considered in the present paper, the autaptic current $I^{\text{aut}} = -g^{\text{aut}}(V(t) - V^{\text{aut}})\Gamma(V(t))$ with $\Gamma(V(t)) = 1/(1 + e^{-\lambda(V(t)-\theta_{\text{aut}})})$ is added to Eq. (1) to form the model with autapse, which is described as follows:

$$\frac{dV}{dt} = V - \frac{V^3}{3} - \omega + I^{\text{aut}}, \tag{10}$$

$$\frac{d\omega}{dt} = \varepsilon(-u + V - S(\omega)), \tag{11}$$

$$\frac{du}{dt} = \mu(u_p + V). \tag{12}$$

$$I^{\text{aut}} = -g^{\text{aut}}(V(t) - V^{\text{aut}})\Gamma(V(t)), \tag{13}$$

$$\Gamma(V(t)) = 1/(1 + e^{-\lambda(V(t)-\theta_{\text{aut}})}) \tag{14}$$

In the present paper, we mainly consider fast autapse. Then, a large value of λ, $\lambda = 30$, to ensure that autapse is fast is considered. For fast autapse, nonzero pulse current appears when $V > \theta_{\text{aut}}$ and zero current appears for $V < \theta_{\text{aut}}$. Considering that the membrane potential of an action potential of the modified FHN model is between -1.87 and 1.89, and θ_{aut} should be a value within the range of the membrane potential of an action potential, a middle value between -1.87 and 1.89 is considered in the present paper. Then, $\theta_{\text{aut}} = 0$ to ensure a relative narrow pulse current is considered in the present paper. In the following sections, I^{aut} is labeled as I_e^{sum} and g^{aut} as g_e^{aut} for the excitatory autapse, and I_i^{aut} and g_i^{aut} for the inhibitory autapse. Due to that the membrane potential V of spiking of the modified FHN model is between -1.87 and 1.89, the autaptic current is excitatory for $V_e^{\text{aut}} = 2$ to ensure the nonnegative values of I_e^{aut} and inhibitory for $V_i^{\text{aut}} = -2$ to ensure the nonpositive values of I_i^{aut}. The modified FHN model with $I^{\text{aut}} = 0$ ($g^{\text{aut}} = 0$) corresponds to the condition without autapse.

Method

The ordinary differential equations were solved by numerical integration method of the fourth-order Runge-Kutta (integration time step: 0.001). A spike is thought to generate if the membrane potential reaches 0 from below. The software XPPAUT 8.071 is used to calculate the bifurcations (Ermentrout 2002).

Results

Bursting behaviors for no autapse ($I^{\text{aut}} = 0$)

When $I^{\text{aut}} = 0$ ($g^{\text{aut}} = 0$), the modified FHN model exhibits bifurcation process with the decrease of u_p, as shown in Fig. 1a and b, which is characterized by the interspike intervals (ISIs) of the firing pattern. Figure 1b is the enlargement of the part within the box of Fig. 1a. The ISI means the time interval between two successive spikes. For example, the period-4 bursting exhibits 4 values of ISI in turn, as shown in Fig. 1c. The ISIs mean the series of ISI, which can be used to characterize bifurcations of ISI, as shown in Fig. 1a and b. For a fixed parameter, 100 ISI values are used.

With the decrease of u_p from $u_p = 0.8$, period-4 bursting changes to period-5 bursting, to period-6 bursting, to period-7 bursting, ..., eventually to period-16 bursting, and to tonic spiking via a shrink. The membrane potentials of period-4 bursting ($u_p = 0.8$), period-6 bursting ($u_p = 0.6$), period-12 bursting ($u_p = 0.4$), and period-16 bursting ($u_p = 0.35$) are shown in Fig. 1c–f, respectively. The membrane potentials with many spikes in a burst ($u_p = 0.345$) and period-1 spiking ($u_p = 0.2$) are shown in Fig. 1g and h, respectively. There is a saddle-homoclinic orbit bifurcation at $u_p \approx 0.808$. The resting state appears when $u_p > 0.8$.

To clearly characterize the detailed dynamics of the periodic bursting, some concepts in a period of bursting are defined, such as the period-8 bursting for $u_p = 0.5$, as shown in Fig. 2. The membrane potential is represented by black curve and the variable u is denoted by blue curve. The 1st to 8th ISIs within a period are defined as $\text{ISI}_{(k)}$ ($k = 1, 2, \cdots, 8$), where k is the sequential number within a period. The maximal value and minimal value of u for the k^{th} ($k = 1, 2, \cdots, 8$) spike within a period are labeled as $u_{(k)}^{\max}$ and $u_{(k)}^{\min}$, respectively. The changes of $\text{ISI}_{(k)}$, $u_{(k)}^{\max}$, and $u_{(k)}^{\min}$ with respect to the sequential number k can be used to characterize the dynamics of the bursting modulated by autapse.

Bursting activities for the excitatory and inhibitory autapses

In the present paper, $u_p = 0.5$ is used as a representative to discuss the effect of autapse on bursting activity. In the absence of autapse ($g_e^{\text{aut}} = g_i^{\text{aut}} = 0$), the spike trains of period-8 bursting (black) for $u_p = 0.5$ and zero autaptic current ($I^{\text{aut}} = 0$, red) are shown in Fig. 3a.

For the excitatory autapse, the period number of bursting decreases with increasing g_e^{aut}, as shown by the left column of Fig. 3. Bursting patterns change from period-7

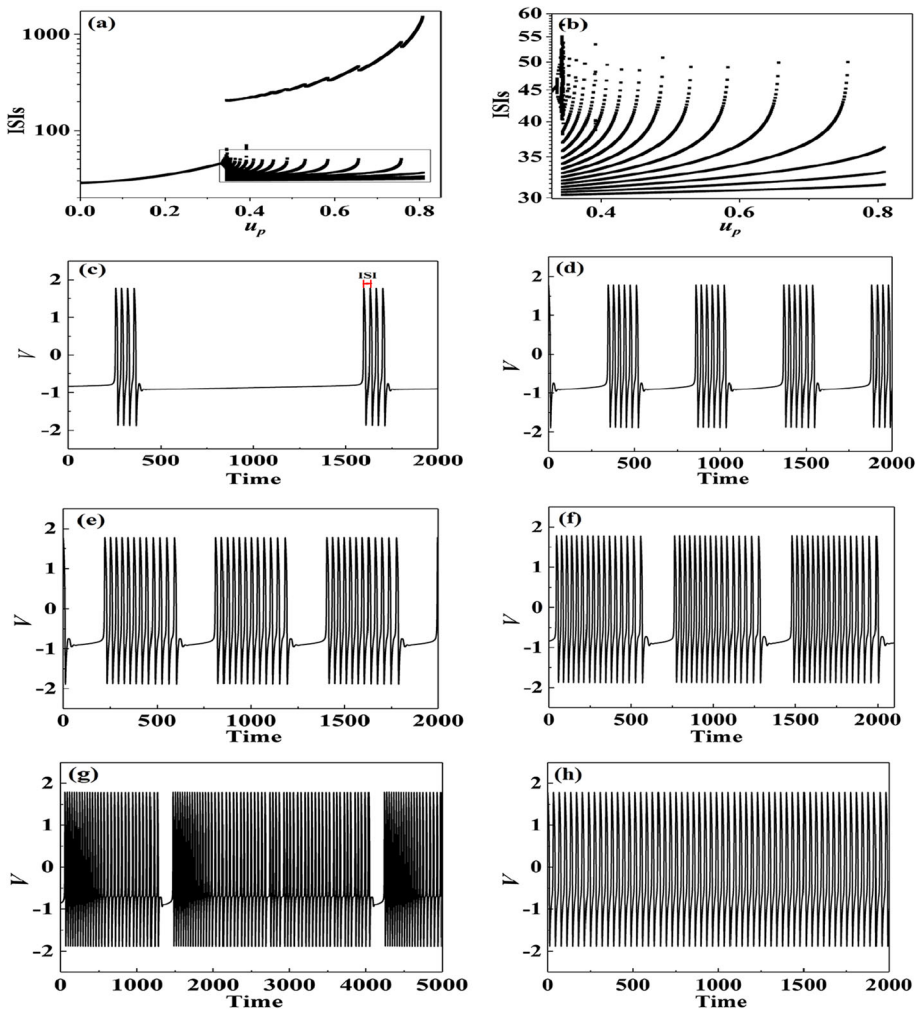

Fig. 1 The dynamics of firing pattern in the modified FHN model without autapse. **a** Bifurcations characterized by ISIs with respect to u_p; **b** The enlargement of the rectangular box in Fig. (a); **c** The period-4 bursting for $u_p = 0.8$; **d** The period-6 bursting for $u_p = 0.6$; **e** The period-12 bursting for $u_p = 0.4$; **f** The period-16 bursting for $u_p = 0.35$; **g** The bursting with many spikes in a burst for $u_p = 0.345$; **h** The period-1 spiking for $u_p = 0.2$

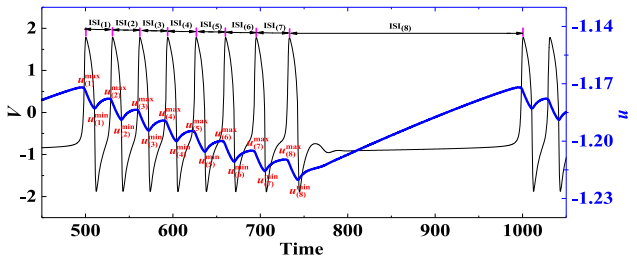

Fig. 2 $\mathrm{ISI}_{(k)}$ and the local maximum ($u^{\max}_{(k)}$) and minimum ($u^{\min}_{(k)}$) values of the slow variable u within a period of period-8 bursting in absence of autapse ($g_e^{aut} = g_i^{aut} = 0$). Membrane potential V and slow variable u are represented by black and blue, and k is the sequential number within a burst ($k = 1, 2, \ldots, 8$)

(g_e^{aut} = 0.2), to period-5 (g_e^{aut} = 0.6), to period-4 (g_e^{aut} = 0.62), as illustrated in Fig. 3b1, c1 and d1, respectively, showing the reduced bursting activities.

For the inhibitory autapse, the period number of bursting increases within a range of g_i^{aut}. Firing pattern changes from period-9 bursting ($g_i^{aut} = 0.05$), to period-10 bursting (g_i^{aut} = 0.18), as illustrated in Fig. 3b2 and c2, respectively. The results indicate that the bursting activity induced by inhibitory autapse is enhanced at first. However, as g_i^{aut} increases to 0.23, the bursting pattern recovers to period-8, as illustrated in Fig. 3d2, showing that strong inhibitory autapse induces the bursting activities reduced again.

For the excitatory autapse, the ISIs (black) of bursting patterns show an inverse period-adding bifurcation process with increasing g_e^{aut}, as illustrated in Fig. 4a. "P8, P7, P6, P5, and P4" represent period-8, period-7, period-6, period-5, and period-4 bursting patterns, respectively, as shown in Fig. 4a. The mean firing frequency (rate) refers to the ratio of the spike number in a period to the time length of the period. The mean firing frequency (red) manifests a decreasing trend, as shown in Fig. 4a. For the inhibitory autapse, the number of spikes per burst is from 8, to 9, to 10, to 9, and to 8 with increasing g_i^{aut}, as illustrated by ISIs (black) and denoted by "P8, P9, and P10" in Fig. 4b. Correspondingly, the firing rate (red) increases at first and then decreases. In the present paper, we mainly emphasize the enhanced bursting activity at low conductance of inhibitory autapse ($g_i^{aut} < 0.18$).

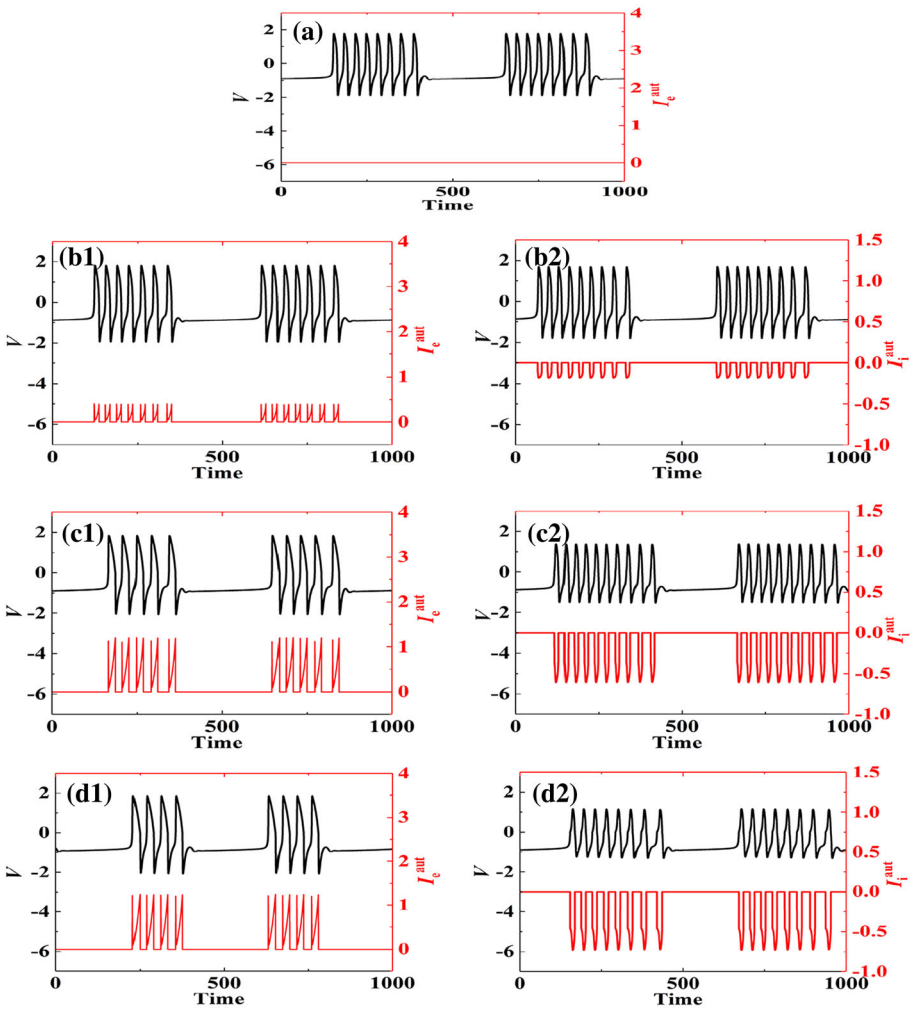

Fig. 3 (Color online) The membrane potential of bursting (black) and the autaptic current (red) for $u_p = 0.5$. **a** Period-8 bursting for $g_e^{aut} = g_i^{aut} = 0$; **b1** Period-7 bursting for $g_e^{aut} = 0.2$; **b2** Period-9 bursting for $g_i^{aut} = 0.05$; **c1** Period-5 bursting for $g_e^{aut} = 0.6$; **c2** Period-10 bursting for $g_i^{aut} = 0.18$; **d1** Period-4 bursting for $g_e^{aut} = 0.62$; **d2** Period-8 bursting for $g_i^{aut} = 0.23$

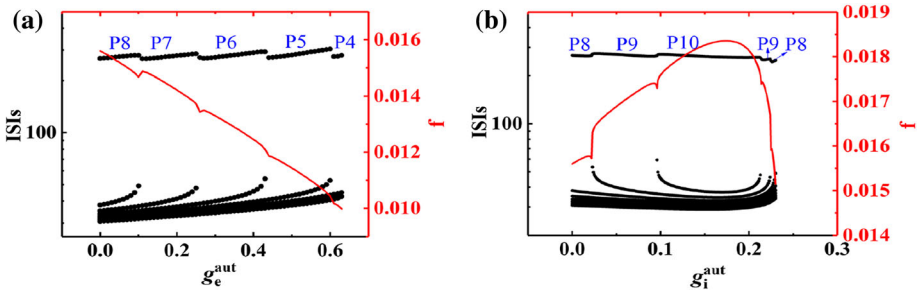

Fig. 4 (Color online) The changes of ISIs (black) and firing rate (red) with respect to the autaptic conductance for $u_p = 0.5$. **a** Excitatory autapse; **b** Inhibitory autapse. "P8, P7, P6, P5, and P4" represent period-8, period-7, period-6, period-5, and period-4 bursting patterns, respectively; "P8, P9, P10" represent period-8, period-9, and period-10 bursting patterns, respectively

As defined in Fig. 2, a period-k bursting has k ISIs labeled as $ISI_{(k)}$ in a period. At different levels of g_e^{aut}, different periodic bursting patterns appear. For example, period-8, period-7, period-6, and period-5 bursting patterns appear for g_e^{aut} = 0, 0.2, 0.4, and 0.6, respectively. Then, there exists 8, 7, 6, and 5 ISIs a in period. the changes of $ISI_{(k)}$ with respect to k (sequential number in a burst) for period-8 (black), period-7 (green), period-6 (red), and period-5 (blue) are depicted in Fig. 5. For the excitatory autapse, the number of ISIs in a period decreases with

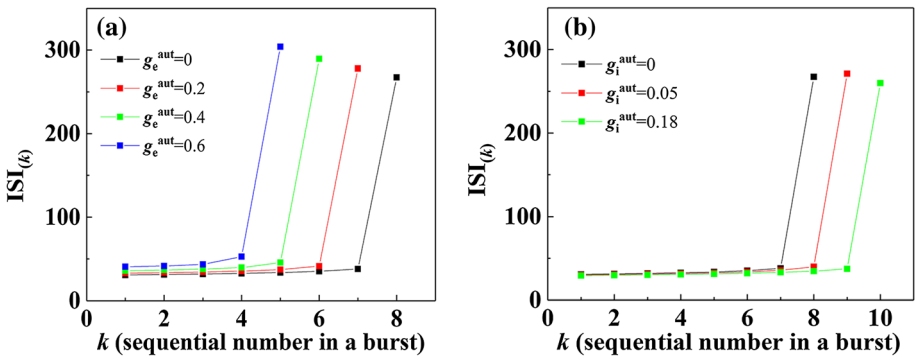

Fig. 5 (Color online) The changes of $ISI_{(k)}$ with respect to the sequential number k of ISIs in a period of bursting induced different types autapse. **a** Excitatory autapse: the black, red, green, and blue represent $g_e^{aut} = 0$, 0.2, 0.4, and 0.6, respectively; **b** Inhibitory autapse: the black, red, and green represent $g_i^{aut} = 0$, 0.05, and 0.18, respectively

increasing g_e^{aut}, as shown in Fig. 5a. Especially, the ISIs corresponding to the same sequential number increase to a certain extent. Therefore, less spikes per burst is the dominant factor to induce the reduced bursting activity. For the inhibitory autapse with small values of g_i^{aut}, the number of ISIs in a period increases with increasing g_i^{aut}, as shown in Fig. 5b, and the ISIs corresponding to the same sequential number decrease to a certain extent, which shows that the change of spike number is the dominant factor of the enhanced bursting activities.

For the excitatory autapse, the firing patterns at higher autaptic conductivities are very different from the bursting patterns without autapse. For the inhibitory autapse, the subthreshold oscillations appear. Then, in the present paper, the membrane voltage behavior at higher autaptic conductivities have been discussed in the Appendix B.

The dynamics of the slow variable *u* of the bursting activity

It is well known that the changes of bursting dynamics are related to the slow variable u. To show the dynamics of the slow variable u, the projections of phase trajectory (u, V) at different values of autaptic conductance are depicted in Fig. 6. The phase trajectory runs along the direction depicted by the arrows. For the period-8 bursting corresponding to $g^{aut} = 0$ (i.e., $g_e^{aut} = g_i^{aut} = 0$), the phase trajectory (u, V) is illustrated in Fig. 6a.

For the excitatory autapse, the trajectory (u, V) of period-7 bursting ($g_e^{aut} = 0.2$) is depicted in Fig. 6b1 and of period-5 bursting ($g_e^{aut} = 0.6$) in Fig. 6c1. The range of u of a burst remains nearly unchanged at different values of g_e^{aut}. For the inhibitory autapse, the trajectories (u, V) of period-9 bursting ($g_i^{aut} = 0.05$) and period-10 bursting ($g_i^{aut} = 0.18$) are shown in Fig. 6b2 and c2, respectively. The range of u of a burst slightly changes with increasing g_i^{aut}. Therefore, the spike number per burst is mainly determined by the width of u between continual spikes. For example, the excitatory autapse, from period-7 (g_e^{aut} = 0.2, Fig. 6b1) to period-5 ($g_e^{aut} = 0.6$, Fig. 6c1), the width of u between continual spikes becomes longer, resulting in less spikes per burst.

The width of *u* between continual spikes for excitatory autapse

For a period-k bursting, the maximal value and minimal value of u in a period of bursting is labeled as $u_{(k)}^{max}$ and $u_{(k)}^{min}$, respectively, as shown in Fig. 2. At different values of g_e^{aut}, the changes of $u_{(k)}^{max}$ and $u_{(k)}^{min}$ with respect to k are illustrated in Fig. 7a1 and b1, respectively. For each g_e^{aut}, the changes of $u_{(k)}^{max}$ and $u_{(k)}^{min}$ exhibit nearly slope lines, such as the black line for $g_e^{aut} = 0$, red line for $g_e^{aut} = 0.2$, and green line for $g_e^{aut} = 0.6$. With increasing g_e^{aut}, the slopes of the lines increase, i.e. the widths of u between continual spikes become longer. Considering that the range of u for a burst is nearly independent of g_e^{aut}, as shown by the left panels of Fig. 6, the increase of width of u between continual spikes leads to less spikes per burst. Similarly, the changes of $u_{(k)}^{min}$ shown in Fig. 7b1 exhibit similar result. Therefore, the increase of width of u between continual spikes with increasing g_e^{aut} is the cause for the less spikes per burst.

The width of *u* between continual spikes for inhibitory autapse

At each of different values of g_i^{aut}, the change of $u_{(k)}^{max}$ and $u_{(k)}^{min}$ with respect to k manifests nearly linear line, as shown by black ($g_i^{aut} = 0$), red ($g_i^{aut} = 0.05$), and green ($g_i^{aut} = 0.18$) in Fig. 7a2 and b2. With increasing g_i^{aut}, the slopes of lines for both $u_{(k)}^{max}$ and $u_{(k)}^{min}$ get more negative, which show that the width of u between continual spikes decreases. This is the cause for the enhanced number of spikes per burst with increasing g_i^{aut}.

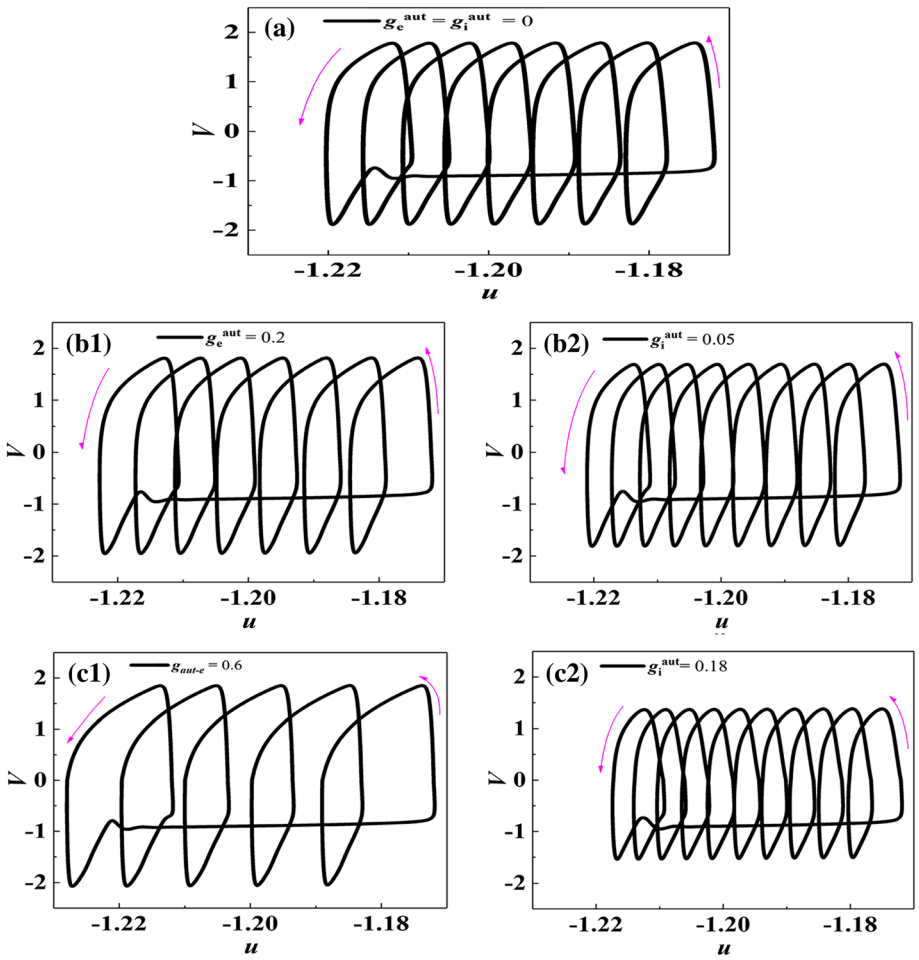

Fig. 6 (Color online) The projections of the phase trajectories (u, V) at different levels of autaptic conductance (corresponding to Fig. 3). **a** Period-8 bursting for $g_e^{aut} = g_i^{aut} = 0$; **b1** Period-7 bursting for $g_e^{aut} = 0.2$; **b2** Period-9 bursting for $g_i^{aut} = 0.05$; **c1** Period-5 bursting for $g_e^{aut} = 0.6$; **c2** Period-10 bursting for $g_i^{aut} = 0.18$. The phase trajectory runs along the direction labeled with arrow

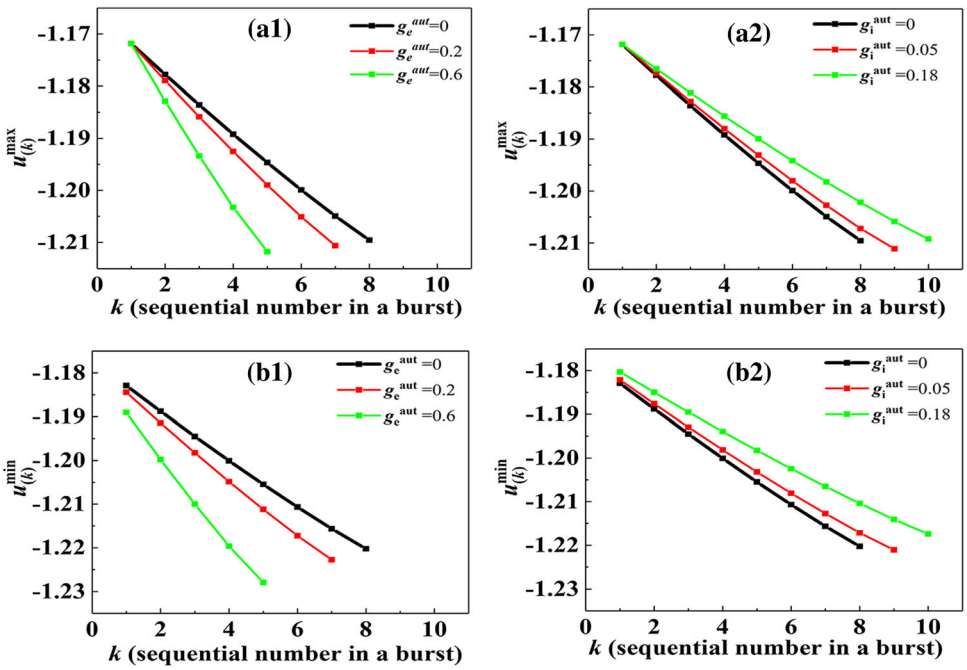

Fig. 7 (Color online) The local maximum ($u_{(k)}^{max}$) and minimum ($u_{(k)}^{min}$) values of the slow variable u at different values of autaptic conductance. $u_{(k)}^{max}$: **a1** Different levels of g_e^{aut}; **a2** Different levels of g_i^{aut}; $u_{(k)}^{min}$: **b1** Different levels of g_e^{aut}; **b2** Different levels of g_i^{aut}. Left: $g_e^{aut} = 0, 0.2$, and 0.6 are represent by black, red, and green, respectively. Right: g_i^{aut} = 0, 0.05, and 0.18 are represented by black, red, and green, respectively

The bifurcations underlying the bursting patterns

The dynamics of the bursting patterns can be acquired by using the fast-slow variable dissection. The equations of the fast subsystem are shown as follows:

$$\frac{dV}{dt} = V - \frac{V^3}{3} - \omega + I^{aut}, \tag{15}$$

$$\frac{d\omega}{dt} = \varepsilon(-u + V - S(\omega)). \tag{16}$$

where u is the bifurcation parameter. The autaptic current I^{aut} is contained in the fast subsystem, which is different from the autapse with time delay (wherein the I^{aut} is not contained in the fast subsystem (Ding and Li 2016)).

The bifurcations of the fast subsystem

For each of the different values of g_e^{aut} and g_i^{aut}, the fast subsystem exhibits a "S"-shaped curve of equilibrium, as depicted in Fig. 8(a1) and (a2), respectively, which contains the upper (unstable focus, dot curve; stable focus, bold curve), middle (saddle, dash curve), and lower (stable node, bold curve) branches. For the excitatory autapse, the black, red, and green curves in Fig. 8a1 represent $g_e^{aut} = 0$, 0.2, and 0.6, respectively. For the inhibitory autapse, the black, red, and green curves in Fig. 8a2 represent $g_i^{aut} = 0$, 0.05, and 0.18, respectively. For each conductance of either autapse, the middle and lower branches intersect to form a saddle-node (fold) bifurcation, which is labeled as SN (bold triangle). A stable limit cycle around the upper branch emerges via a Hopf bifurcation (bold dot), and evolves to the left with increasing g_e^{aut} or g_i^{aut}, as illustrated in Fig. 8b1 and b2. The spiking behavior corresponds to the stable limit cycle.

The dynamics of the spiking

Fig. 8c1 and c2 represent the local enlargement of Fig. 8b1 and b2 around the SH (saddle-homoclinic orbit) point, respectively. For the excitatory autapse, at different values of autaptic conductance, the SH points have nearly equaling u values, which means that the stable limit cycles disappear at a nearly fixed u value, as shown in Fig. 8c1. For the inhibitory autapse, the SH points move to right slightly with increasing autaptic conductance, i.e., the disappearance of the stable limit cycles exhibits a slightly elevation of u value, as shown in Fig. 8c2.

V_{max} and V_{min} of the spiking change with respect to the autaptic conductance. For the excitatory autapse, V_{max} values increase slightly with increasing g_e^{aut}, whereas V_{min} values decrease slightly, as shown in Fig. 8b1 and c1, resulting in the increased amplitude of the spiking. For the inhibitory autapse, V_{max} values decrease with increasing g_i^{aut}, whereas V_{min} values elevate, as illustrated in Fig. 8b2 and c2, resulting in the reduced amplitude of the spiking.

The "Fold/Big Homoclinic" bursting pattern

For each panel of Fig. 8, the corresponding projection of phase trajectory of the bursting is superimposed to the plane (u, V) to form Fig. 9. The (u, V) trajectory (bold solid curve) for $g_e^{aut} = 0$ (black) is depicted in Fig. 9a. For the excitatory autapse, the (u, V) trajectories (bold solid curves) for $g_e^{aut} = 0.2$ (red) and 0.6 (green) are illustrated in Fig. 9b1 and c1, respectively. For the inhibitory autapse, the (u, V) trajectories of the burstings (bold solid curves) for $g_i^{aut} = 0.05$ (red) and 0.18 (green) are illustrated in Fig. 9b2 and c2, respectively. In each panel of Fig. 9, the burst starts from the fold (SN) bifurcation and terminates at the SH bifurcation (a big saddle-homoclinic orbit), showing a "Fold/Big Homoclinic" pattern (More details please refer to the Appendix A)(Izhikevich 2000).

Changes of bursting dynamics with respect to autaptic conductance

For the excitatory autapse, fold (SN) point and SH point are nearly fixed and independent of g_e^{aut}. Then, the ranges of u values for the burst are nearly fixed. As shown in Figs. 6 and 9, the width of u between successive spikes becomes wider with the increase of g_e^{aut}, which is the cause for less spikes per burst and lower firing rate with increasing g_e^{aut}. For the different levels of g_i^{aut}, the fold (SN) points are nearly fixed. SH point are nearly fixed at small g_i^{aut}. However, u values of SH points slightly increase with the increase of g_i^{aut} at strong g_i^{aut}. Thus, with increasing g_i^{aut}, the range of u value for the burst decreases slightly. The width of u between successive spikes becomes narrower with the increase of g_i^{aut} (Figs. 6 and 9). Therefore, more spikes per burst appear ($g_i^{aut} = 0.05$ and $g_i^{aut} = 0.18$), resulting in the enhancement of bursting activity.

ISI of spiking of the fast subsystem

ISI of spiking is another important characteristic of the fast subsystem. For the excitatory autapse, the ISI for $g_e^{aut} = 0$ (black), 0.2 (red), 0.6 (green) is shown in Fig. 10a1. For a fixed g_e^{aut}, ISI decreases with respect to the increase of u. For different values of g_e^{aut}, the stronger the g_e^{aut} is, the longer the ISI value is. For the inhibitory autapse, the ISI of spiking for $g_i^{aut} = 0$ (black), $g_i^{aut} = 0.05$ (red), and $g_i^{aut} = 0.18$ (green) are depicted in Fig. 10a2. For a fixed g_i^{aut}, ISI decreases with respect to the increase of u. For a fixed u

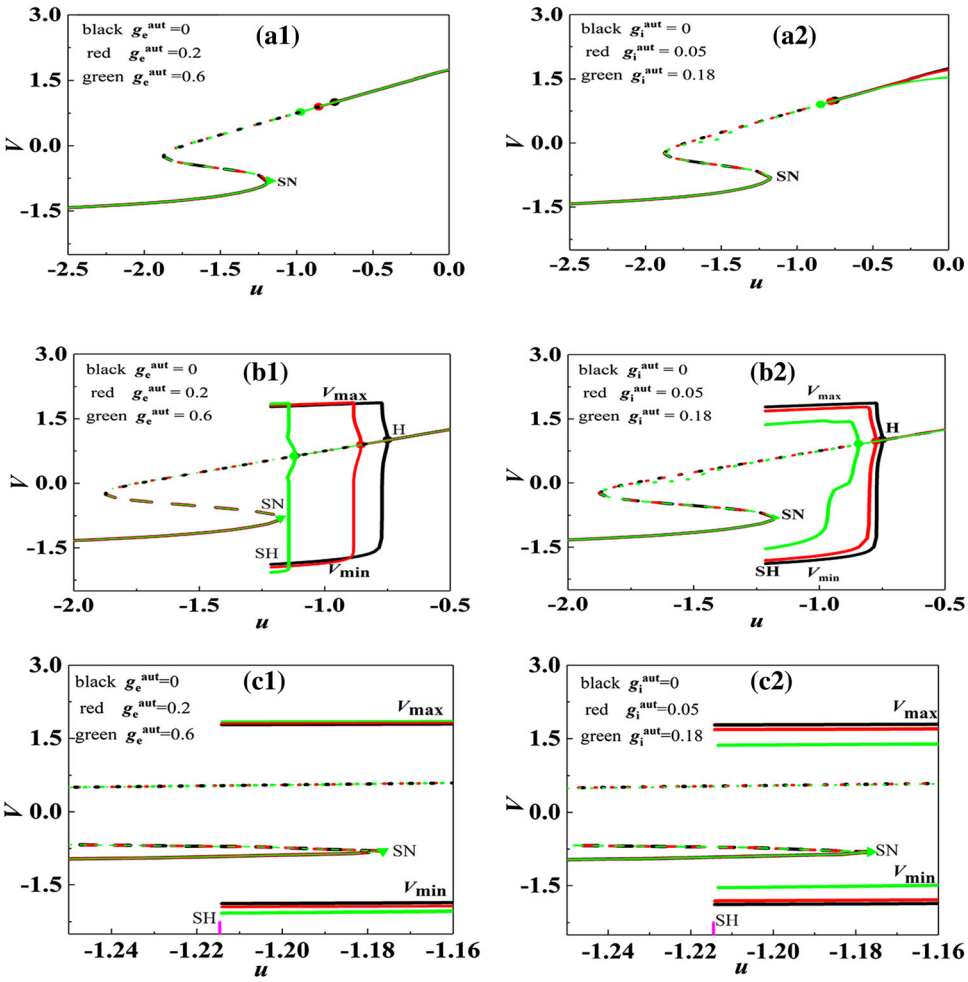

Fig. 8 (Color online) The bifurcations of the fast subsystem respect to different values of autaptic conductance. The bifurcations of equilibrium points: **a1** Excitatory autapse; **a2** Inhibitory autapse; The bifurcations of the limit cycles are added to the first row: **b1** Excitatory autapse; **b2** Inhibitory autapse; The enlargement: **c1** corresponding to Fig. (b1); **c2** corresponding to Fig. (b2). The "S"-shaped curves represent the equilibrium point curves at different values of autapse. SN (bold triangle), SH (pink line), and H (bold dot) represent the saddle-node, saddle-homoclinic orbit, and Hopf bifurcations, respectively. V_{max} (V_{min}) represents the maximal (minimal) value of the stable limit cycle, respectively. Excitatory autapse: black, red, and green represent g_e^{aut} = 0, 0.2, and 0.6; Inhibitory autapse: black, red, and green represent g_i^{aut} = 0, 0.05, 0.18

value, from g_i^{aut} = 0 (black), to 0.05 (red), and to 0.18 (green), ISI decreases. The distribution of ISI values (color) on the plane (u, g_e^{aut}) for the excitatory autapse is illustrated in Fig. 10b1. The left boundary of the color region corresponds to the SH point, and the vertical pink line represents the SN point. At a fixed value of u, the stronger the g_e^{aut} is, the longer the ISI value is. For the inhibitory autapse, the distributions of ISI on the plane (u, g_i^{aut}) is illustrated in Fig. 10b2. At a fixed value of u, the value of ISI becomes shorter with the increase of g_i^{aut}. If u is below the SH point, the membrane voltage behavior of the fast subsystem exhibits resting state.

Such distributions can be used to explain the changes of width of u between continual spikes within a burst of the bursting patterns with respect to g_e^{aut} or g_i^{aut}. For the excitatory autapse, the basic idea is as follows: for a bursting pattern with a stronger g_e^{aut}, a larger width of u between continual spikes within a burst is induced by the longer period of spiking at the stronger g_e^{aut}, which is the cause that less spikes per burst are evoked between the SN and SH points at the stronger g_e^{aut}. Such a result can be found from Fig. 11a, which represents the u value (black) at the peak of k^{th} spike of the bursting superimposed to the distribution of ISI values (color) on the plane (u, g_e^{aut}). The width of u between two continual spikes increases with increasing g_e^{aut}, resulting in less spikes per burst. If u_{max} or u_{min} instead of u value at the spike peak is used, the result is similar (not shown here to avoid possible repetitions). The result for the inhibitory autapse is shown in Fig. 11b. The ISI values of spiking decrease with increasing g_i^{aut}, resulting in short width of u between two continual spikes within a burst. Therefore, more spikes per burst appear with increasing g_i^{aut}.

Current dynamics of the fast subsystem

As mentioned above, in the fast subsystem, three measures for the stable limit cycle, the range of u, the amplitude related to V_{min} and V_{max}, and the ISI of spiking, play important roles in the bursting activity modulated by the autapse. In the present section, the current mechanisms for the changes of V_{min} and V_{max} and the ISI of spiking are

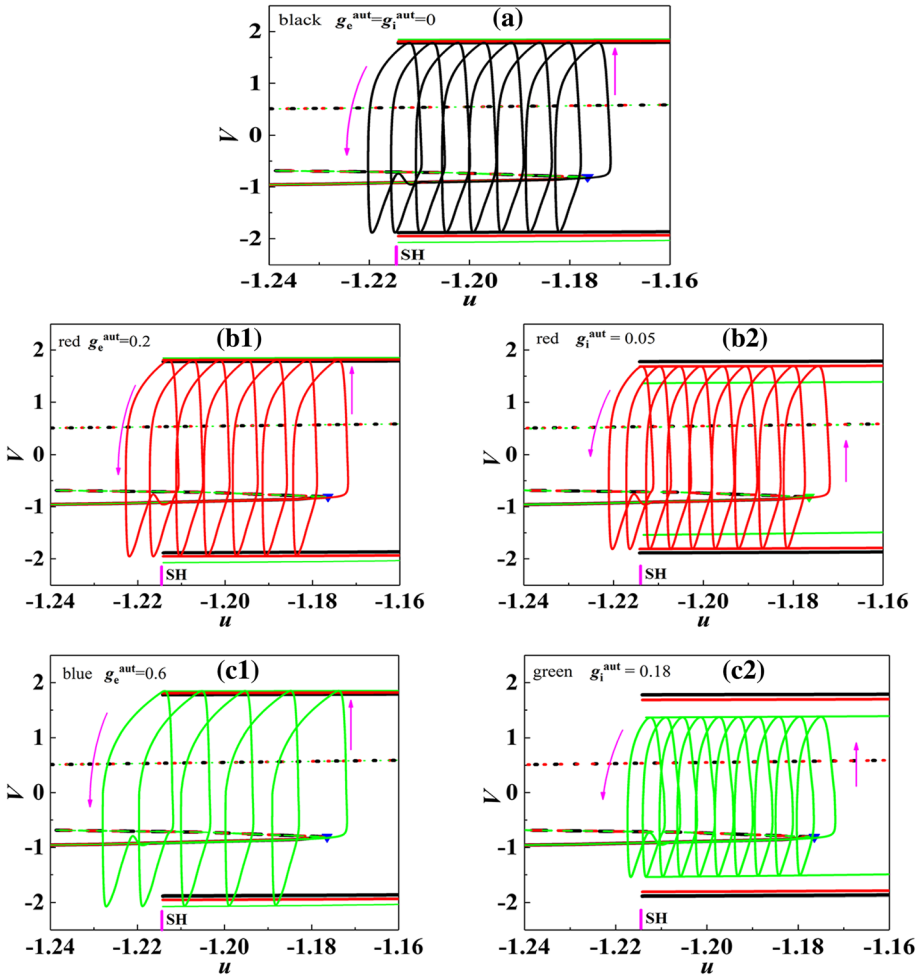

Fig. 9 (Color online) The phase trajectory (u, V) of bursting plotted with bifurcations of the fast subsystem at different values of autaptic conductance (Fig. 8). **a** Period-8 bursting for $g_e^{aut} = g_i^{aut} = 0$; **b1** Period-7 bursting for $g_e^{aut} = 0.2$; **b2** Period-9 bursting for $g_i^{aut} = 0.05$; **c1** Period-5 bursting for $g_e^{aut} = 0.6$; **c2** Period-10 bursting for $g_i^{aut} = 0.18$. The arrows represent the direction of the phase trajectory of bursting, and the blue bold triangle represents the SN point. SH represent the saddle-homoclinic orbit bifurcation

acquired. The relationships between V and the currents such as the I^{aut} (autaptic current), the total current ($I^{sum} = \frac{dV}{dt} = V - \frac{V^3}{3} - \omega + I^{aut}$), and other current exclusive the autaptic current ($I^{sum} - I^{aut} = V - \frac{V^3}{3} - \omega$) are studied.

As shown in Fig. 8 (V_{max} and V_{min}) and Fig. 10 (ISI), for a fixed u value locating between the fold (SN) bifurcation and the saddle-homoclinic orbit (SH) bifurcation, the changing trends of V_{max}, V_{min}, and ISI of the fast subsystem with respect to g^{aut} are the same. Then, any a fixed u value between the SN bifurcation and SH bifurcation can be used as a representative to show the dynamics of spiking. Without losing generality, $u = -1.2$ is chosen as a representative in the present paper.

Spiking behavior before and after application of autapse to the fast subsystem

In the present section, spiking (black) corresponding to the stale limit cycle for $u = -1.2$ is chosen as a representative, which corresponds to the behavior before the pink arrows depicted in Fig. 12a and b. An excitatory autapse with $g_e^{aut} = 0.2$ (red) and $g_e^{aut} = 0.6$ (green) is respectively applied at the pink arrow, as illustrated in Fig. 12a. With increasing g_e^{aut}, V_{max} becomes larger and V_{min} becomes lower, which is consistent with Fig. 8, and the ISI of spiking becomes longer, i.e. the pulse of the action potential becomes longer, which is consistent with Fig. 10. An inhibitory autapse with $g_i^{aut} = 0.05$ (red) and $g_i^{aut} = 0.18$ (green) is respectively applied at the pink arrow, as depicted in Fig. 12b. With increasing g_i^{aut} from 0 to 0.18, V_{max} decreases and V_{min} elevates, which is consistent with Fig. 8. From $g_i^{aut} = 0$, to 0.05 (red), and to 0.18 (green), the ISI of spiking decreases slightly, which is consistent with Fig. 10.

The relationship between the membrane potential (V) and the autaptic current $I^{aut} = -g^{aut}(V(t) - V^{aut})\Gamma(V(t))$ containing $\Gamma(V(t)) = 1/(1 + e^{-\lambda(V(t)-\theta_{aut})})$ and the threshold of autapse θ_{aut} has been clearly introduced in the Section model and method. $\theta_{aut} = 0$ is used in the present paper. The excitatory current exhibits positive pulse when $V > \theta_{aut}$ and zero value when $V < \theta_{aut}$, showing that the excitatory autaptic current plays a role around the peak of

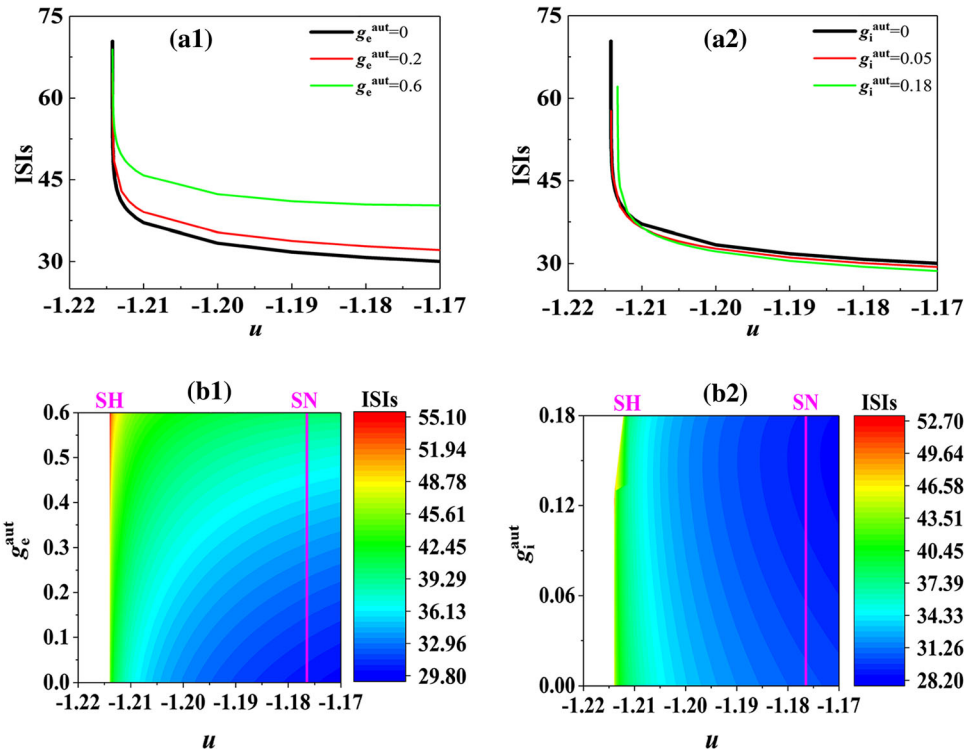

Fig. 10 (Color online) ISIs of spiking. Changes of ISIs of spiking with respect to u at different values of autaptic conductance: **a1** Excitatory autapse: black, red, and green represent g_e^{aut} = 0, 0.2, and 0.4, respectively; **a2** Inhibitory autapse: black, red, and green represent g_i^{aut} = 0, 0.05, and 0.18; The distributions of ISI values (color) on the parameter plane for different types of autapse. **b1** The plane (u, g_e^{aut}) for the excitatory autapse; **b2** The plane (u, g_i^{aut}) for the inhibitory autapse. The left boundary of the color region represents the SH point and the vertical pink line represents the SN point

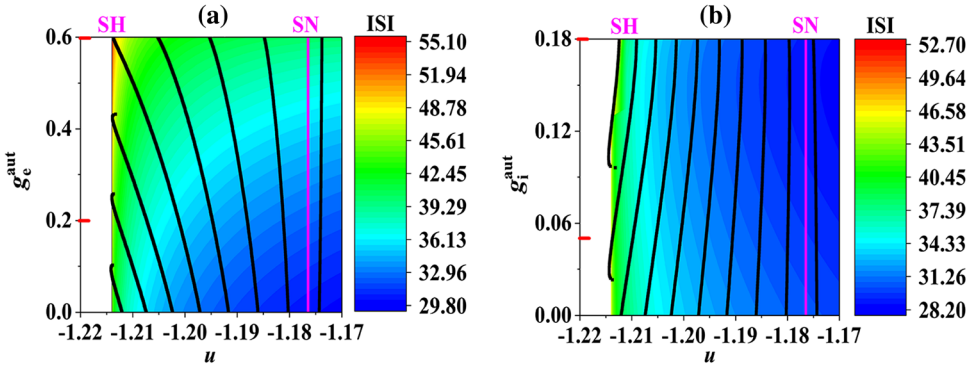

Fig. 11 (Color online) The u value at peak of spike of the bursting (black) plotted with the values (color) of ISI of spiking on the parameter plane for different types of autapse. **a** The plane (u, g_e^{aut}) for the excitatory autapse; The horizontal red lines represent g_e^{aut} = 0.2 and 0.6 for Fig. 9. **b** The plane (u, g_i^{aut}) for the inhibitory autapse. The horizontal red lines represent g_i^{aut} = 0.05 and 0.18 for Fig. 9

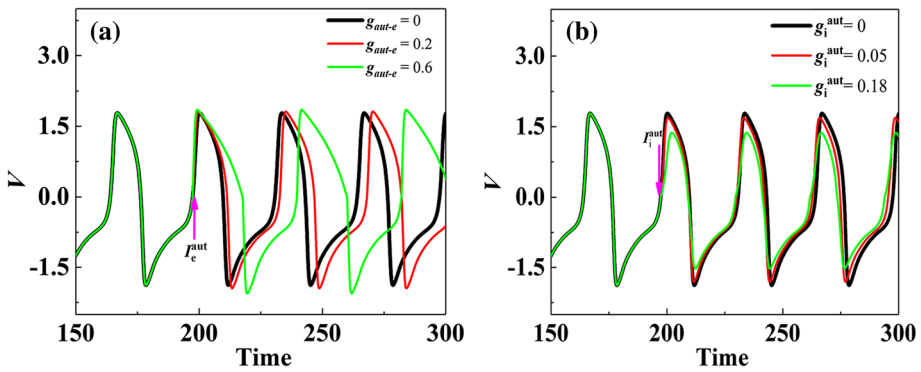

Fig. 12 (Color online) Spike trains of the fast subsystem at u = −1.2. Autapse with different values of conductance is respectively applied at the pink arrow. **a** Excitatory autapse: g_e^{aut} = 0 (black), 0.2 (red), 0.6 (green); **b** Inhibitory autapse: g_i^{aut} = 0 (black), 0.05 (red), and 0.18 (green)

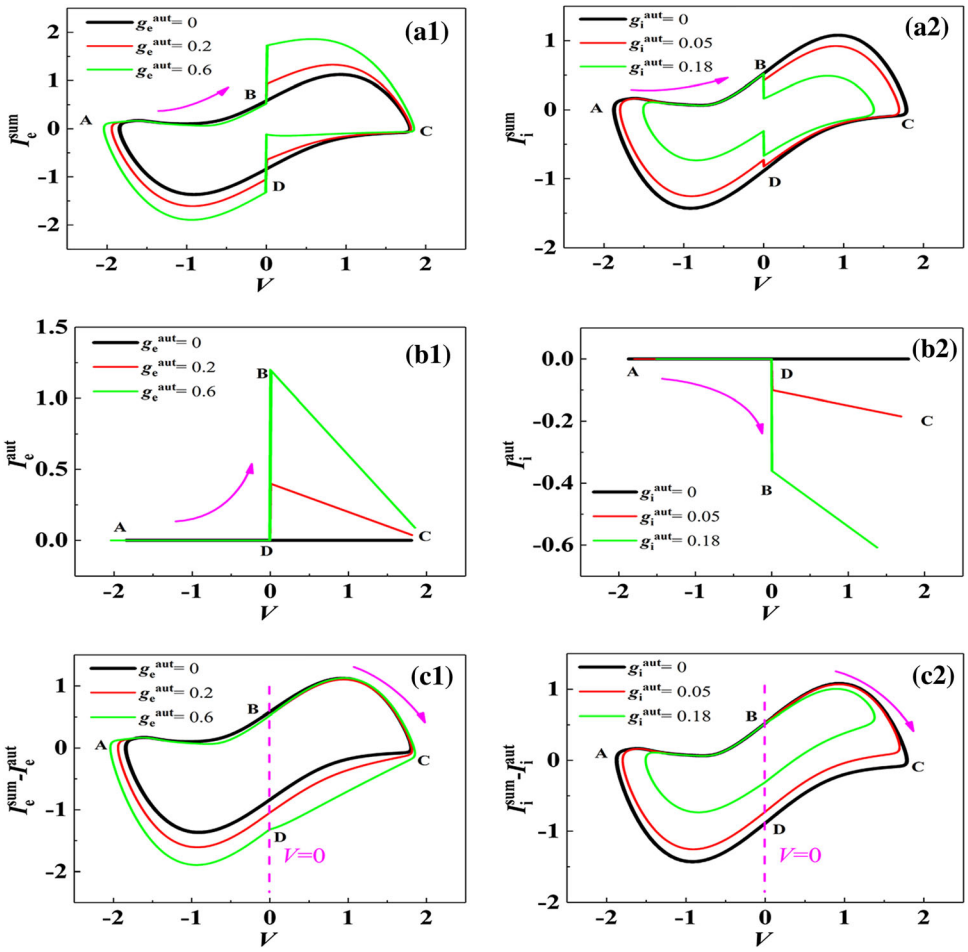

Fig. 13 (Color online) Currents vs V at different values of autaptic conductance of the fast subsystem for $u = -1.2$. **a1** I_e^{sum}; **a2** I_i^{sum}; **b1** I_e^{aut}; **b2** I_i^{aut}; **c1** $I_e^{sum} - I_e^{aut}$; **c2** $I_i^{sum} - I_i^{aut}$. Left column: the excitatory autapse. Black, red, and green represent $g_e^{aut} = 0$, 0.2, and 0.6, respectively; Right column: the inhibitory autapse. Black, red, and green represent $g_i^{aut} = 0$, 0.05, and 0.18, respectively

the action potential or spike to enhance the amplitude of the action potential. The larger the g_e^{aut} is, the stronger the I_e^{aut} is, and the higher the amplitude of the action potential is. For the inhibitory autapse, the inhibitory autaptic current exhibits negative pulse when $V > \theta_{aut}$ and zero value when $V < \theta_{aut}$, i.e., the inhibitory autaptic current plays a role around the peak of the action potential or spike to reduce the amplitude of action potential. The larger the g_i^{aut} is, the stronger the I_i^{aut} is, and the lower the amplitude is. The autaptic current of the fast subsystem mainly plays a role during the peak of the action potential ($V > \theta_{aut}$, i.e., 0), differing from the well-known slow autaptic current, which plays a role following the peak of the action potential. It is the fast dynamics of the fast autaptic current that induces the paradoxical phenomenon. The slow autaptic current should induce common phenomenon of bursting activity, which should be studied in future.

The current mechanism for the excitatory autapse

To explain the amplitudes of spikes at different values of g_e^{aut}, the total current $I_e^{sum} = \frac{dV}{dt} = V - \frac{V^3}{3} - \omega + I^{aut}$ is considered. The trajectories (V, I_e^{sum}) at $g_e^{aut} = 0$ (black), 0.2 (red), and 0.6 (green) are shown in Fig. 13a1. For convenience, four phases are considered, which are the minimal value of V (phase A), $V = 0$ on the ascending branch of spike (phase B), maximal value of V (phase C), and $V = 0$ on the descending branch of spike (phase D). $V = 0$ corresponds to the threshold of the autapse $\theta_{aut} = 0$. The detailed results are as follows:

From phase B to C (the ascending branch of action potential with $V > 0$): with increasing g_e^{aut}, I_e^{sum} becomes larger, resulting in larger maximal value of V at phase C, i.e., the higher V_{max}.

From phase C to D (the descending branch of action potential with $V > 0$): the stronger the g_e^{aut} is, the weaker the I_e^{sum} is, resulting in slower repolarization of V, i.e., the pulse of action potential becomes longer, which is consistent with that of Fig. 12.

From phase D to A (the descending branch of action potential with $V < 0$): with increasing g_e^{aut}, I_e^{sum} becomes more polarization, resulting in the lower maximal value of V at phase A, i.e., the lower V_{min}.

From phase A to B (the ascending branch of action potential with $V < 0$): I_e^{sum} between different values of g_e^{aut} exhibits little difference, resulting in the larger maximal value of V at phase C, i.e., the higher V_{max}. Therefore, the trajectories (V, I_e^{sum}) manifest little difference.

The total current $I_e^{sum} = \frac{dV}{dt} = V - \frac{V^3}{3} - \omega + I^{aut}$ contains two parts, the autaptic current (I_e^{aut}) and other current exclusive the autaptic current ($I_e^{sum} - I_e^{aut}$). The roles of two parts of current are considered. The trajectories of (V, I_e^{aut}) at $g_e^{aut} = 0$ (black), 0.2 (red), and 0.6 (green) are shown in Fig. 13b1, and the trajectories of (V, $I_e^{sum} - I_e^{aut}$) are shown in Fig. 13c1. It should be noticed that across phase B or D, I_e^{sum} changes drastically due to that V runs across $\theta_{aut} = 0$. The detailed results are as follows:

From phase B to C (the ascending branch of action potential with $V > 0$): The autaptic current I_e^{aut} is positive due to $V > 0$. With increasing g_e^{aut}, positive I_e^{aut} becomes larger, while $I_e^{sum} - I_e^{aut}$ remains nearly unchanged. Therefore, a higher V_{max} appearing at the stronger g_e^{aut} is mainly evoked by the autaptic current I_e^{aut}.

From phase C to D (the descending branch of action potential with $V > 0$): With increasing g_e^{aut}, positive I_e^{aut} becomes larger, and negative $I_e^{sum} - I_e^{aut}$ becomes stronger. As a result, negative I_e^{sum} becomes weaker. Therefore, $I_e^{sum} - I_e^{aut}$ determines the sign of I_e^{sum} , and I_e^{aut} determines the strength of I_e^{sum}. For a fixed g_e^{aut}, the larger the I_e^{aut} is, the higher value the I_e^{sum} is. The result shows that the autaptic current I_e^{aut} plays a dominant role, compared with $I_e^{sum} - I_e^{aut}$.

From phase D to A (the descending branch of action potential with $V < 0$): The autaptic current I_e^{aut} approximates zero due to $V < 0$. With increasing g_e^{aut}, I_e^{aut} remains nearly unchanged to be 0, and the negative $I_e^{sum} - I_e^{aut}$ becomes stronger, resulting in lower I_e^{sum}, which shows that $I_e^{sum} - I_e^{aut}$ plays a dominant role.

From phase A to B (the ascending branch of action potential with $V < 0$): For different values of g_e^{aut}, the autaptic current I_e^{aut} is 0, and $I_e^{sum} - I_e^{aut}$ exhibits little difference.

The current mechanism for the inhibitory autapse

The trajectories of (V, I_i^{sum}), (V, I_i^{aut}), and (V, $I_i^{sum} - I_i^{aut}$) at $g_i^{aut} = 0$ (black), 0.05 (red), and 0.18 (green) are shown in Fig. 13a2, b2, and c2, respectively. Different from the excitatory autapse, I_i^{aut} for the inhibitory autapse when $V > 0$ is negative. The detailed results are as follows:

From phase B to C (the ascending branch of action potential with $V > 0$): With increasing g_i^{aut}, positive $I_i^{sum} - I_i^{aut}$ becomes lower, and negative I_i^{aut} becomes stronger, resulting in a lower positive I_i^{sum}. Therefore, V_{max} at phase C becomes lower.

From phase C to D (the descending branch of action potential with $V > 0$): The stronger the g_i^{aut} is, the more negative the I_i^{aut} is, and the higher the positive $I_i^{sum} - I_i^{aut}$ is, resulting in a slightly lower level of the negative I_i^{sum}. Therefore, the period of the spiking slightly decreases.

From phase D to A (the descending branch of action potential with $V < 0$): The autaptic current I_i^{aut} approximates zero due to $V < \theta_{aut} = 0$. With increasing g_i^{aut}, negative $I_i^{sum} - I_i^{aut}$ and I_i^{sum} are elevated, resulting in an elevated V_{min}.

From phase A to B (the ascending branch of action potential with $V < 0$): I_i^{aut} approximates zero, and $I_i^{sum} - I_i^{aut}$ between different values of g_i^{aut} exhibits little difference. Therefore, I_i^{sum} between different values of g_i^{aut} exhibits little difference, resulting in little difference of the trajectory (V, I_i^{sum}) between different values of g_i^{aut}.

Summary

The distinction of the dynamics of bursting of full system and spiking of fast subsystem between the excitatory and inhibitory autapse is shown in Table 1. For the excitatory autapse, the excitatory autaptic current is positive around the peak of the action potential of the fast subsystem. Then, the larger excitatory autapse induces the larger positive current around the peak of the spike. The spike amplitude enhances and the repolarization becomes weak, resulting in longer ISI of spiking. The longer ISI induces wider width of slow variable u between two successive spikes. Due to that the burst width of the slow variable u remains unchanged, corresponding to the unchanged bifurcation points of fold (SN) and saddle-homoclinic orbit (SH), the number of spikes within a burst becomes smaller, which presents the cause for the reduced number of spikes per burst and firing frequency for the excitatory autapse.

For the inhibitory autapse, the inhibitory autaptic current is negative around the peak of the action potential of the fast subsystem. Then, the larger inhibitory autapse induces the stronger negative current around the peak of the spike. The spike amplitude reduces, resulting in shorter ISI of spiking. The shorter ISI induces narrower width of slow variable u between two successive spikes. Due to that the burst width of the slow variable u remains nearly unchanged, corresponding to that the bifurcation points of fold (SN) and saddle-homoclinic orbit (SH) remains nearly unchanged, then, the number of spikes with a burst becomes larger, which presents the cause for the enhanced number of spikes per burst and firing frequency for the inhibitory autapse.

Table 1 Summary for the distinction of bursting and spiking of fast subsystem between the excitatory and inhibitory autapse

	Dynamics of bursting or spiking	Excitatory autapse	Inhibitory autapse
Bursting (Full system)	Number of spikes per burst	Reduced	Enhanced
	Firing frequency	Reduced	Enhanced
Fast-slow variable dissection	Bifurcation points (burst width)	Unchanged	Nearly unchanged
	Width of slow variable u between two successive spikes	Enhanced	Reduced
Spiking(Fast subsystem)	ISI of spiking	Enhanced	Reduced
	Autaptic current(Depolarization and repolarization)	Enhanced (Positive)	Reduced (Negative)
	Amplitude of spike	Enhanced	Reduced

Conclusion and discussion

In the real nervous system, bursting regulated by the inhibitory or excitatory effects plays important roles in multiple aspects (Glass 2001; Ma et al. 2021; Yang et al. 2018; Mondal et al. 2019; Lisman 1997; Braun et al. 1994; Gu and Pan 2015; Duan et al. 2020; Yang et al. 2021; Xu et al. 2020). Therefore, it is of great significance to reveal the dynamics and regulation mechanism of different bursting patterns for the nonlinear science and neuroscience. Recent studies have revealed the mechanisms of paradoxical phenomena in the neural electrical activities under the actions of various regulatory factors, especially the self-feedback/autapse, which enrich the connotation of neurodynamics (Beiderbeck et al. 2018; Li et al. 2019; Wu and Gu 2020; Cao et al. 2021; Wang et al. 2020; Cao et al. 2018). In the present paper, it is revealed that both fast excitatory and inhibitory self-feedbacks/autapses can respectively induce the paradoxical phenomena for the "Fold/Big Homoclinic" bursting pattern, which have significances in the following aspects.

Firstly, the types of bursting for paradoxical phenomenon are extended. In previous studies (Li et al. 2019; Wang et al. 2020; Lu et al. 2021), for the "Fold/(small)Homoclinic" bursting (small is added to be distinguished with big, and the burst terminates via a saddle-homoclinic orbit bifurcation with a small amplitude of homoclinic orbit), paradoxical phenomena are induced by excitatory or inhibitory autapses. In the present paper, the "Fold/Big Homoclinic" bursting with burst terminating via a saddle-homoclinic orbit bifurcation with a large amplitude of homoclinic orbit is considered (Please refer to the Appendix A). Both excitatory and inhibitory autapses respectively induce paradoxical phenomena for the "Fold/Big Homoclinic" bursting, showing a new example of the paradoxical phenomenon.

Secondly, a novel nonlinear mechanism for the paradoxical phenomenon is given, which is based on the dynamics of the fast subsystem. In the present paper, both the Fold and the Big Homoclinic orbit bifurcation points change little with changing the autaptic conductance, resulting in that u (slow variable) range of a burst is nearly fixed. Under the action of autaptic current, the ISI of spiking of the fast subsystem changes, which induces different widths of u between spikes within a burst. Excitatory autapse induces large width of u for a spike, resulting in less spikes per burst. Inhibitory autapse induces small range of u for a spike, leading to the enhanced spike number per burst. Such results are different from those of previous studies on other bursting patterns (Li et al. 2019; Cao et al. 2021; Wang et al. 2020; Cao et al. 2018; Ding and Li 2016; Li et al. 2021; Lu et al. 2021), wherein the values of bifurcation points or types of bifurcation change.

Finally, paradoxical phenomena and regulatory mechanisms are extended. The paradoxical phenomena in the present paper are different from not only those induced by autapse without time delay in previous studies (Li et al. 2019; Wang et al. 2020; Li et al. 2021; Lu et al. 2021) but also with time delay for bursting (Cao et al. 2021, 2018; Ding and Li 2016) and spiking (Zhao et al. 2020a, b). It is found that inhibitory autapse can enhance bursting activity or excitatory autapse can reduce bursting activity at appropriate time delays (Zhao et al. 2020b; Ding and Li 2016). The time delay can change the action phase of autapse current pulse applied to the fast subsystem (Cao et al. 2018; Ding and Li 2016). The influence of time delay is important, due to that the time delay of autapse must be crucial. The excitatory autapse with relatively large time delay can induce less spikes per burst (paradoxical phenomenon) of the bursting in the modified FitzHugh–Nagumo model, while with relatively time delay induce more spikes per burst (the common phenomenon) (Cao et al. 2021) . If the pulse plays a role at a suitable phase, the paradoxical phenomenon is induced.

Reviewing the literatures, it can be found that the paradoxical phenomena are dependent on the firing patterns, excitation or inhibition effects, diverse measures such as the stimulation, autapse, memristor, and ionic current (Zhao et al. 2020b; Ding and Li 2016; Hua et al. 2020; Chay 1985; Li et al. 2021; Lu et al. 2021; Wang and Rinzel 1992; Jia 2018; Xu et al. 2020; Wang and Shi 2020). The paradoxical phenomena induced by the autapse

in the present paper are dependent of neruon model and autapse model, compared with Refs (Wang et al. 2020; Li et al. 2021). In addition, the model used in the present paper is not based on ion channels, then, the practical significance of these paradoxical phenomena awaits future experimental demonstration. In future, the paradoxical phenomena and underlying mechanism should be studied comprehensively and deeply. In the present paper, a theoretical model of fast autapse (Wang and Rinzel 1992) is studied. The autaptic current does not exhibit exponential decay following a spike and induces paradoxical phenomenon of bursting activity. Another important synapse model, the exponential decay model (Elson et al. 2002; Moss and Smart 2001; Barbero-Castillo et al. 2021), is also widely studied. The autaptic current exhibits exponential decay following a spike, which may have different effects on the bursting activity. Furthermore, fast autapse and slow autapse have different effects on the depolarization block near a Hopf bifurcation (Zhao et al. 2016; Jia 2018). Therefore, the effect of slow synapse or autapse on bursting activity should be investigated in the future.

Appendix A: Big homoclinic orbit bifurcation

For $g_e^{aut} = g_i^{aut} = 0$, a big homoclinic orbit and a saddle-homoclinic orbit (SH) bifurcation appear at $u = u_2 \approx -1.21419$, as shown in Fig. 14a. For $u = u_1 = -1.22$ ($u <-$

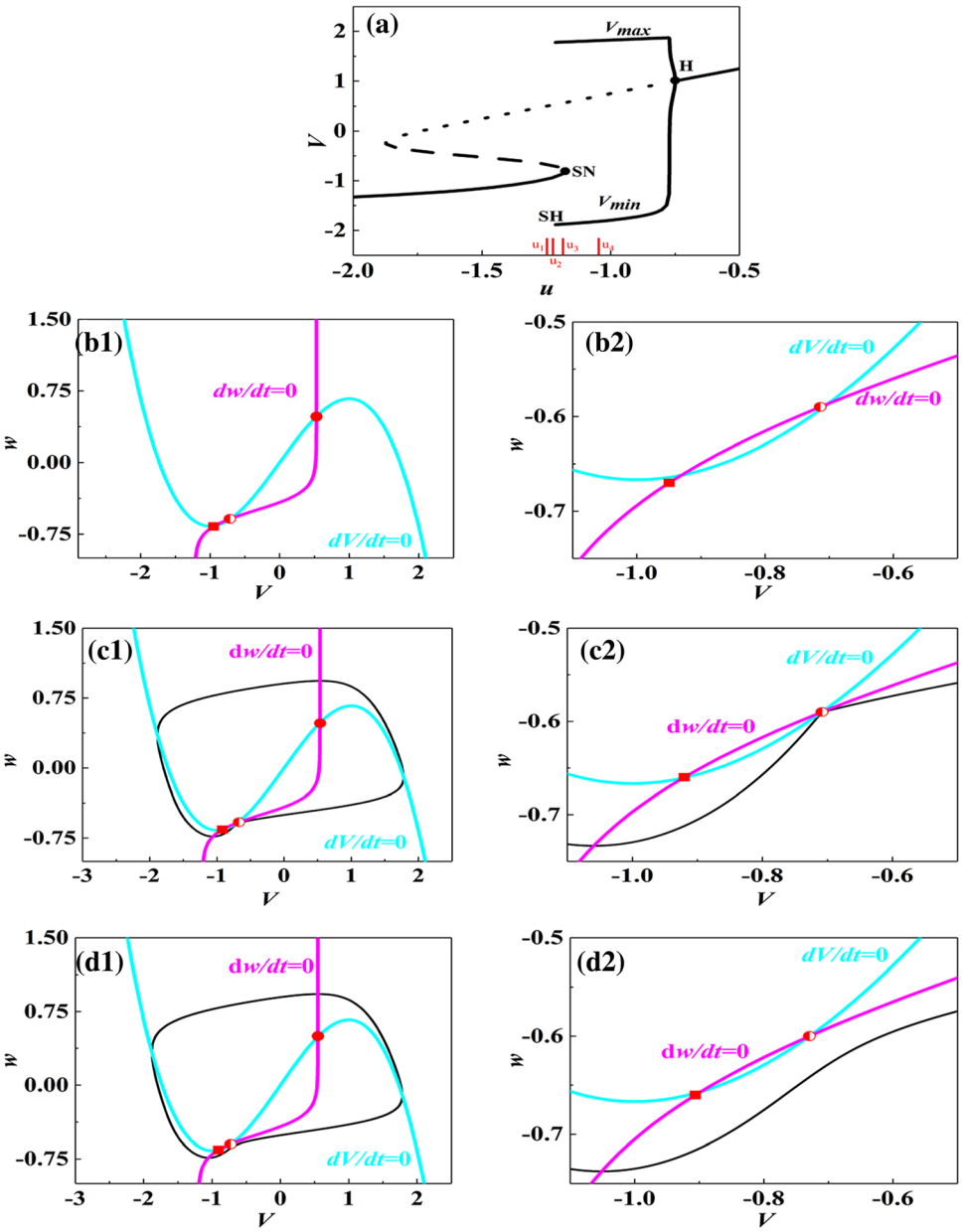

Fig. 14 (Color online) The dynamics related to saddle-homoclinic orbit bifurcation and a big homoclinic orbit in the modified FHN bifurcation for $u_p = 0.5$ and $g_e^{aut} = g_i^{aut} = 0$. **a** Bifurcation diagram of V with respect to u; SH represents a saddle-homoclinic orbit bifurcation; **b1** Dynamics of stable node at $u = u_1 = -1.22$ in phase plane. **b2** Partial enlargement around the saddle and node in Fig. 14b1; **c1** Dynamics of a big homoclinic orbit in phase plane at $u = u_2 = -1.21419$. **c2** Partial enlargement around the saddle in Fig. 14c1; **d1** Dynamics of coexistence of stable node and limit cycle in phase plane for $u = u_3 = -1.2$. **d2** Partial enlargement around the lower part of the limit cycle in Fig. 14d1. The cyan curve and the magenta curve represent the nullclines of V ($dV/dt = 0$) and w ($dw/dt = 0$), respectively. The red dot, red square, and red half bold dot represent the unstable focus, stable node, and saddle, respectively

1.21419), the dynamics in phase plane is shown in Fig. 14b1 and b2. Fig. 14b2 is the enlargement around the node and saddle in Fig. 14b1. The blue curve and the magenta curve represent the nullclines of V ($dV/dt = 0$) and w ($dw/dt = 0$), respectively. There is a stable node (red square), a saddle (red and white dot), and an unstable focus (red dot). For $u = u_2 \approx -1.21419$, a big homoclinic obit (black solid line) appears, which begins from and terminates at the saddle and contains the stable node and unstable focus, as shown in Fig. 14c1 and c2. Figure 14c2 is the enlargement around the saddle in Fig. 14c1. When $-1.17800 > u > -1.21419$, for example, $u = u_3 = -1.2$, the big homoclinic orbit disappears and changes to a stable limit cycle containing the unstable focus, saddle, and a stable node, as shown in Fig. 14d1 and d2. Figure 14d2 is the enlargement around the lower part of the limit cycle in Fig. 14d1.

Appendix B: The membrane voltage behavior at higher autaptic conductivities

The membrane voltage behavior at higher autaptic conductivities for the excitatory autapse are shown in Fig. 15. With increasing g_e^{aut}, the duration of burst increase and spikes within a burst decreases. Due to that the bursting patterns are different from those of the lower g_e^{aut}, we do not further investigate these bursting patterns and the dynamical mechanism underlying the bursting patterns.

For the inhibitory autapse, when $g_i^{aut} > 0.23$, the membrane voltage behavior exhibits the subthreshold oscillations (the resting state), such as $g_i^{aut} = 0.24$ (Fig. 16).

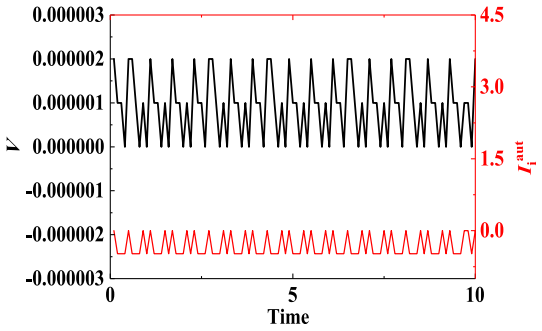

Fig. 16 The membrane potential (black) and autaptic current (red) for inhibitory autapse $g_i^{aut} = 0.24$

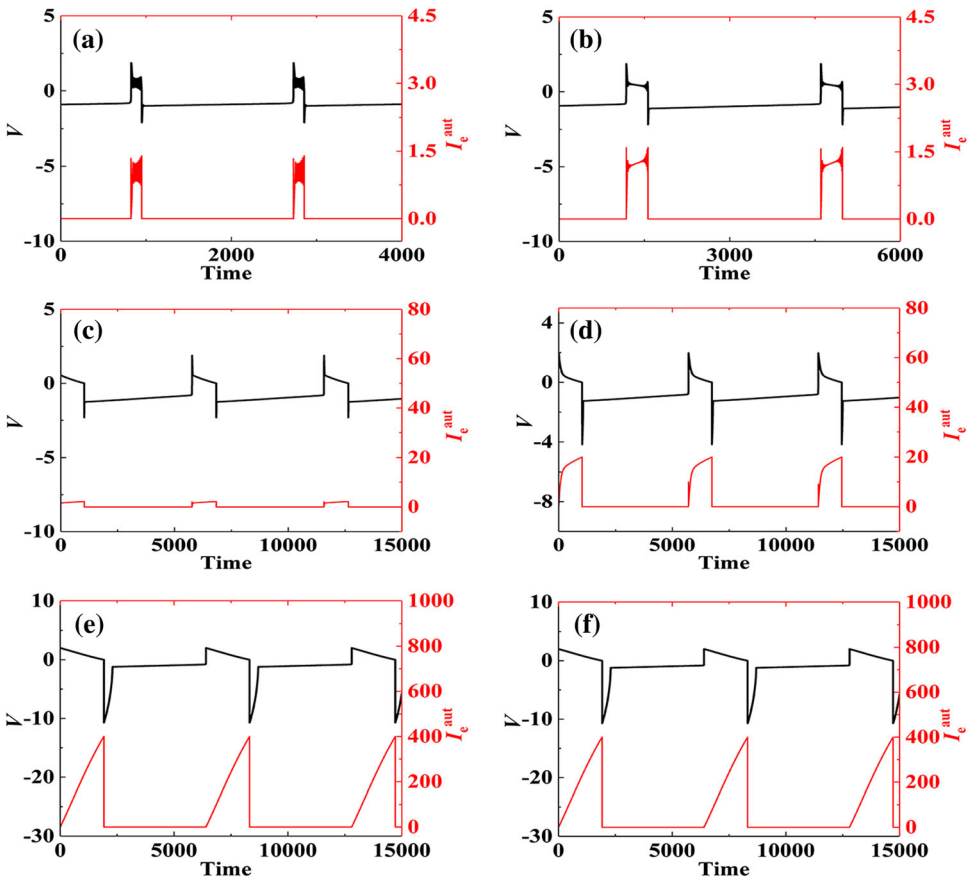

Fig. 15 The membrane potential (black) and autaptic current (red) for the excitatory autapse. **a** $g_e^{aut} = 0.7$; **b** $g_e^{aut} = 0.8$; **c** $g_e^{aut} = 1.1$; **d** $g_e^{aut} = 10$; **e** $g_e^{aut} = 100$; **f** $g_e^{aut} = 200$

Acknowledgements This work was supported by the National Natural Science Foundation of China (Grant Numbers:12162002, 11872276,11762001), the Program for Young Talents of Science and Technology in Universities of Inner Mongolia Autonomous Region (Grant Number: NJYT-20-A09), Natural Science Foundation of Inner Mongolia Autonomous Region of China (Grant Number: 2021MS01016), the Innovation Team of Complex Analysis and Nonlinear Dynamic Systems of Chifeng University (Grant Number: cfxykycxtd202005) and the Program for Key Laboratory Construction of Chifeng University (Grant Number: CFXYZD202004).

Author Contributions Y.L., H.G. conceived the experiments, C.Q., Y.L., H.G., and Y.Y. conducted the experiments, C.Q., Y.L., H.G., and Y.Y. analyzed the results, C.Q. and Y.L. written the paper. All authors reviewed the manuscript.

Data Availibility Statement The datasets generated during and/or analysed during the current study are available from the corresponding author on reasonable request.

Declarations

Conflict of interest The authors declare no competing financial interests.

References

Auffenberg E, Hedrich UB, Barbieri R, Miely D, Groschup B, Wuttke TV, Vogel N, Lührs P, Zanardi I, Bertelli S, Spielmann N, Gailus-Durner V, Fuchs H, Hrabě de Angelis M, Pusch M, Dichgans M, Lerche H, Gavazzo P, Plesnila N, Freilinger T (2021) Hyperexcitable interneurons trigger cortical spreading depression in an Scn1a migraine model. J Clin Invest 131(21):e142202. https://doi.org/10.1172/JCI142202

Bacci A, Huguenard JR (2006) Enhancement of spike-timing precision by autaptic transmission in neocortical inhibitory interneurons. Neuron 49:119–130. https://doi.org/10.1016/j.neuron.2005.12.014

Bacci A, Huguenard JR, Prince DA (2003) Functional autaptic neurotransmission in fast-spiking interneurons: a novel form of feedback inhibition in the neocortex. J Neurosci 23:859–866. https://doi.org/10.1523/JNEUROSCI.23-03-00859.2003

Barbero-Castillo A, Mateos-Aparicio P, Dalla PL, Camassa A, Perez-Mendez L, Sanchez-Vives MV (2021) Impact of GABAA and GABAB inhibition on cortical dynamics and perturbational complexity during synchronous and desynchronized states. J Neurosci 41:5029–5044. https://doi.org/10.1523/JNEUROSCI.1837-20.2021

Baysal V, Erkan E, Yilmaz E (2021) Impacts of autapse on chaotic resonance in single neurons and small-world neuronal networks. Philos Trans A Math Phys Eng Sci 379(2198):20200237. https://doi.org/10.1098/rsta.2020.0237

Beiderbeck B, Myoga MH, Müller N, Callan AR, Friauf E, Grothe B, Pecka M (2018) Precisely timed inhibition facilitates action potential firing for spatial coding in the auditory brainstem. Nat Commun 9:1771. https://doi.org/10.1038/s41467-018-04210-y2018

Braun HA, Wissing H, Schäfer K, Hirsch MC (1994) Oscillation and noise determine signal transduction in shark multimodal sensory cells. Nature 367:270–273. https://doi.org/10.1038/367270a0

Cao B, Guan LN, Gu HG (2018) Bifurcation mechanism of not increase but decrease of spike number within a neural burst induced by excitatory effect. Acta Phys Sin 67:240502. https://doi.org/10.7498/aps.67.20181675 (**in Chinese**)

Cao B, Gu HG, Li YY (2021) Delayed excitatory self-feedback induces negative responses of complex neuronal bursting patterns. Chin Phys B 30:050502. https://doi.org/10.1088/1674-1056/abcfa9

Carlos FP, Ubirakitan MM, Rodrigues MCA, Aguilar-Domingo M, Herrera-Gutiérrez E, Gómez-Amor J, Copelli M, Carelli PV, Matias FS (2020) Anticipated synchronization in human EEG data: unidirectional causality with negative phase lag. Phys Rev E 102(3–1):032216. https://doi.org/10.1103/PhysRevE.102.032216

Cazalets JR, Cournil I, Geffard M, Moulins M (1987) Suppression of oscillatory activity in crustacean pyloric neurons: implication of GABAergic inputs. J Neurosci 7(9):2884–2893. https://doi.org/10.1523/JNEUROSCI.07-09-02884.1987

Chay TR (1985) Chaos in a three-variable model of an excitable cell. Physica D 16:233–242. https://doi.org/10.1016/0167-2789(85)90060-0

Chever O, Zerimech S, Scalmani P, Lemaire L, Pizzamiglio L, Loucif A, Ayrault M, Krupa M, Desroches M, Duprat F, Léna I, Cestèle S, Mantegazza M (2021) Initiation of migraine-related cortical spreading depolarization by hyperactivity of GABAergic neurons and NaV1.1 channels. J Clin Invest 131(21):e142203. https://doi.org/10.1172/JCI142203

Cobb SR, Halasy K, Vida I, Nyiri G, Tamas G, Buhl EH, Somogyi P (1997) Synaptic effects of identified interneurons innervating both interneurons and pyramidal cells in the rat hippocampus. Neuroscience 79:629–648. https://doi.org/10.1016/S0306-4522(97)00055-9

Cymbalyuk GS, Gaudry Q, Masino MA, Calabrese RL (2002) Bursting in leech heart interneurons: cell-autonomous and network-based mechanisms. J Neurosci 22(24):10580–10592. https://doi.org/10.1523/JNEUROSCI.22-24-10580.2002

Debanne D, Campanac E, Bialowas A, Carlier E, Alcaraz G (2011) Axon physiology. Physiol Rev 91(2):555–602. https://doi.org/10.1152/physrev.00048.2009

Deleuze C, Bhumbra GS, Pazienti A, Lourenco J, Mailhes C, Aguirre A, Beato M, Bacci A (2019) Strong preference for autaptic self-connectivity of neocortical PV interneurons facilitates their tuning to γ-oscillations. PLoS Biol 17:e3000419. https://doi.org/10.1371/journal.pbio.3000419

Ding XL, Li YY (2016) Period-adding bifurcation of neural firings induced by inhibitory autapses with time-delay. Acta Phys Sin 65:210502. https://doi.org/10.7498/aps.65.210502 (**in Chinese**)

Ding XL, Jia B, Li YY, Gu HG (2021) Enhancement of coherence resonance induced by inhibitory autapse in Hodgkin–Huxley model. Int J Mod Phys B 35:2150110. https://doi.org/10.1142/S0217979221501101

Dodla R, Rinzel J (2006) Enhanced neuronal response induced by fast inhibition. Phys Rev E 73:010903. https://doi.org/10.1103/PhysRevE.73.01090

Dodla R, Svirskis G, Rinzel J (2006) Well-timed, brief inhibition can promote spiking: postinhibitory facilitation. J Neurophysiol 95:2664–2677. https://doi.org/10.1152/jn.00752.2005

Duan LX, Liang WJ, Ji WC, Xi HG (2020) Bifurcation patterns of bursting within pre-Bötzinger complex and their control. Int J Bifurcat Chaos 13:2050192. https://doi.org/10.1142/S0218127420501928

Duan LX, Liang TT, Zhao YQ, Xi HG (2021) Multi-time scale dynamics of mixed depolarization block bursting. Nonlinear Dyn 103:1043–1053. https://doi.org/10.1007/s11071-020-05744-x

Elson RC, Selverston AI, Abarbanel HDI, Rabinovich MI (2002) Inhibitory synchronization of bursting in biological neurons: dependence on synaptic time constant. J Neurophysiol 88:1166–1176. https://doi.org/10.1152/jn.2002.88.3.1166

Elson RC, Selverston AI, Abarbanel HDI et al (2002) Inhibitory synchronization of bursting in biological neurons: dependence on synaptic time constant. J Neurophysiol 88(3):1166–1176. https://doi.org/10.1152/jn.2002.88.3.1166

Ermentrout B (2002) Simulating, analyzing, and animating dynamical systems: a guide to XPPAUT for researchers and students. SIAM, Philadelphia

Ge MY, Xu Y, Zhang ZK, Peng YX, Kang WJ, Yang LJ, Jia Y (2018) Autaptic modulation-induced neuronal electrical activities and wave propagation on network under electromagnetic induction. Eur Phys J Spec Top 227:799–809. https://doi.org/10.1140/epjst/e2018-700141-7

Ge MY, Jia Y, Xu Y, Lu LL, Wang RW, Zhao YJ (2019) Wave propagation and synchronization induced by chemical autapse in chain Hindmarsh–Rose neural network. Appl Math Comput 352:136–145. https://doi.org/10.1016/j.amc.2019.01.059

Glass L (2001) Synchronization and rhythmic processes in physiology. Nature 410:277–284. https://doi.org/10.1038/35065745

Goldwyn JH, Slabe BR, Travers JB, Terman D (2018) Gain control with A-type potassium current: IA as a switch between divisive and subtractive inhibition. PLoS Comput Biol 14:e1006292. https://doi.org/10.1371/journal.pcbi.1006292

Gu HG, Pan BB (2015) A four-dimensional neuronal model to describe the complex nonlinear dynamics observed in the firing patterns of a sciatic nerve chronic constriction injury model. Nonlinear Dyn 81:2107–2126. https://doi.org/10.1007/s11071-015-2129-7

Gu HG, Pan BB (2015) Identification of neural firing patterns, frequency and temporal coding mechanisms in individual aortic baroreceptors. Front Comput Neurosci 9:108. https://doi.org/10.3389/fncom.2015.00108

Gu XC, Han F, Wang ZJ (2021) Dependency analysis of frequency and strength of gamma oscillations on input difference between excitatory and inhibitory neurons. Cogn Neurodyn 15:501–515. https://doi.org/10.1007/s11571-020-09622-5

Guo DQ, Chen MM, Perc M, Wu SD, Xia C, Zhang YS, Xu P, Xia Y, Yao DZ (2016) Firing regulation of fast-spiking interneurons by autaptic inhibition. Europhys Lett 114:30001. https://doi.org/10.1209/0295-5075/114/30001

Hua HT, Lu B, Gu HG (2020) Nonlinear mechanism of excitatory autapse-inducedreduction or enhancement of firing frequency of neuronal bursting. Acta Phys Sin 69(9):090502. https://doi.org/10.7498/aps.69.20191709 (**in Chinese**)

Izhikevich EM (2000) Neural excitability, spiking and bursting. Int J Bifurcat Chaos 10:1171. https://doi.org/10.1142/S0218127400000840

Izhikevich EM, Desai MS, Walcott EC, Hoppensteadt FC (2003) Bursts as a unit of neural information: selective communication via resonance. Trends Neurosci 26:161–167. https://doi.org/10.1016/S0166-2236(03)00034-1

Jia Bing (2018) Negative feedback mediated by fast inhibitory autapse enhances neuronal oscillations near a Hopf bifurcation point. Int J Bifurcat Chaos 28(2):1850030. https://doi.org/10.1142/S021812741850030X

Jia B, Wu YC, He D, Guo BH, Xue L (2018) Dynamics of transitions from anti-phase to multiple in-phase synchronizations in inhibitory coupled bursting neurons. Nonlinear Dyn 93:1599–1618. https://doi.org/10.1007/s11071-018-4279-x

Jia YB, Gu HG, Li YY, Ding XL (2021) Inhibitory autapses enhance coherence resonance of a neuronal network. Commun Nonlinear Sci Numer Simul 95:105643. https://doi.org/10.1016/j.cnsns.2020.105643

Kim SY, Lim W (2020) Effect of interpopulation spike-timing-dependent plasticity on synchronized rhythms in neuronal networks with inhibitory and excitatory populations. Cogn Neurodyn 14:535–567. https://doi.org/10.1007/s11571-020-09580-y

Li YY, Gu HG, Ding XL (2019) Bifurcations of enhanced neuronal bursting activities induced by the negative current mediated by inhibitory autapse. Nonlinear Dyn 97:2091–2105. https://doi.org/10.1007/s11071-019-05106-2

Li YY, Gu HG, Jia B, Ding XL (2021) The nonlinear mechanism for the same responses of neuronal bursting to opposite self-feedback modulations of autapse. Sci China Ser E Technol Sci 64:1459–1471. https://doi.org/10.1007/s11431-020-1753-y

Lisman JE (1997) Bursts as a unit of neural information: making unreliable synapses reliable. Trends Neurosci 20(1):38–43. https://doi.org/10.1016/S0166-2236(96)10070-9

Liu YR, Liu SQ (2020) Firing patterns of the CA1 pyramidal neuron with geometric singular perturbation: a model study. Int J Mod Phys B 34(32):2050316. https://doi.org/10.1142/S0217979220503166

Liu YR, Liu SQ, Zhan FB, Zhang XH (2020) Firing patterns of the modified Hodgkin–Huxley models subject to Taylor's formula. Physica A 547:124405. https://doi.org/10.1016/j.physa.2020.124405

Lu B, Gu HG, Wang XJ, Hua HT (2021) Paradoxical enhancement of neuronal bursting response to negative feedback of autapse and the nonlinear mechanism. Chaos Solitons Fractals 145:110817. https://doi.org/10.1016/j.chaos.2021.110817

Ma J, Song XL, Tang J, Wang CN (2015) Wave emitting and propagation induced by autapse in a forward feedback neuronal network. Neurocomputing 167:378–389. https://doi.org/10.1016/j.neucom.2015.04.056

Ma KH, Gu HG, Zhao ZG (2021) Fast-slow variable dissection with two slow variables: a case study on bifurcations underlying bursting for seizure and spreading depression. Int J Bifurcat Chaos 31:2150096. https://doi.org/10.1142/S0218127421500966

Matias FS, Carelli PV, Mirasso CR, Copelli M (2011) Anticipated synchronization in a biologically plausible model of neuronal motifs. Phys Rev E 84:021922. https://doi.org/10.1103/PhysRevE.84.021922

Matias FS, Carelli PV, Mirasso CR, Copelli M (2015) Self-organized near-zero-lag synchronization induced by spike-timing dependent plasticity in cortical populations. PLoS ONE 10(10):e04. https://doi.org/10.1371/journal.pone.0140504

Mondal A, Upadhyay RK, Ma J, Yadav BK, Sharma SK, Mondal A (2019) Bifurcation analysis and diverse firing activities of a modified excitable neuron model. Cogn Neurodyn 13:393–407. https://doi.org/10.1007/s11571-019-09526-z

Moss SJ, Smart TG (2001) Constructing inhibitory synapses. Nature Rev Neurosci 2:240–250. https://doi.org/10.1038/35067500

Negro CAD, Hsiao CF, Chandler SH, Garfinkel A (1998) Evidence for a novel bursting mechanism in rodent trigeminal neurons. Biophys J 75:174–182. https://doi.org/10.1016/S0006-3495(98)77504-6

Rubin JE, Terman DH (2000) Geometric analysis of population rhythms in synaptically coupled neuronal networks. Neural Comput 12:597–645. https://doi.org/10.1162/089976600300015727

Saada R, Miller N, Hurwitz I, Susswein AJ (2009) Autaptic excitation elicits persistent activity and a plateau potential in a neuron of known behavioral function. Curr Biol 19:479–484. https://doi.org/10.1016/j.cub.2009.01.060

Satterlie RA (1985) Reciprocal inhibition and postinhibitory rebound produce reverberation in a locomotor pattern generator. Science 229:402–404. https://doi.org/10.1126/science.229.4711.402

Song XL, Wang HT, Chen Y (2019) Autapse-induced firing patterns transitions in the Morris-Lecar neuron model. Nonlinear Dyn 96:2341–2350. https://doi.org/10.1007/s11071-019-04925-7

Tamás G, Buhl EH, Somogyi P (1997) Massive autaptic self-innervation of GABAergic neurons in cat visual cortex. J Neurosci 17:6352–6364. https://doi.org/10.1523/JNEUROSCI.17-16-06352.1997

Tikidji-Hamburyan RA, Martinez JJ, White JA, Canavier CC (2015) Resonant interneurons can increase robustness of gamma oscillations. J Neurosci 35:15682–15695. https://doi.org/10.1523/JNEUROSCI.2601-15.2015

Uzun R, Yilmaz E, Ozer M (2017) Effects of autapse and ion channel block on the collective firing activity of Newman–Watts small-world neuronal networks. Physica A 486:386–396. https://doi.org/10.1016/j.physa.2017.05.049

Uzuntarla M, Torres JJ, Calim A, Barreto E (2019) Synchronization-induced spike termination in networks of bistable neurons. Neural Netw 110:131–140. https://doi.org/10.1016/j.neunet.2018.11.007

Van Vreeswijk C, Abbott LF, Bard Ermentrout G (1994) When inhibition not excitation synchronizes neural firing. J Comput Neurosci 1:313–321. https://doi.org/10.1007/BF00961879

Vida I, Bartos M, Jonas P (2006) Shunting inhibition improves robustness of gamma oscillations in hippocampal interneuron networks by homogenizing firing rates. Neuron 49:107–117. https://doi.org/10.1016/j.neuron.2005.11.036

Wang XJ, Buzsöki G (1996) Gamma oscillation by synaptic inhibition in a hippocampal interneuronal network model. J Neurosci 16:6402–6413. https://doi.org/10.1523/JNEUROSCI.16-20-06402.1996

Wang XJ, Rinzel J (1992) Alternating and synchronous rhythms in reciprocally inhibitory model neurons. Neural Comput 4:84–97. https://doi.org/10.1162/neco.1992.4.1.84

Wang ZL, Shi XR (2020) Electric activities of time-delay memristive neuron disturbed by Gaussian white noise. Cogn Neurodyn 14:115–124. https://doi.org/10.1007/s11571-019-09549-6

Wang QY, Murks A, Perc M, Lu QS (2011) Taming desynchronized bursting with delays in the Macaque cortical network. Chin Phys B 20(4):040504. https://doi.org/10.1088/1674-1056/20/4/040504

Wang HT, Ma J, Chen YL, Chen Y (2014) Effect of an autapse on the firing pattern transition in a bursting neuron. Commun Nonlinear Sci Numer Simul 19:3242–3254. https://doi.org/10.1016/j.cnsns.2014.02.018

Wang XJ, Gu HG, Lu B (2020) Paradoxical reduction and the bifurcations of neuronal bursting activity modulated by positive self-feedback. Nonlinear Dyn 101:2383–2399. https://doi.org/10.1007/s11071-020-05913-y

Wu FQ, Gu HG (2020) Bifurcations of negative responses to positive feedback current mediated by memristor in a neuron model with bursting patterns. Int J Bifurcat Chaos 30:2030009. https://doi.org/10.1142/S0218127420300098

Xu Y, Ying HP, Jia Y, Ma J, Hayat T (2017) Autaptic regulation of electrical activities in neuron under electromagnetic induction. Sci Rep 7:43452. https://doi.org/10.1038/srep43452

Xu Y, Liu MH, Zhu ZG, Ma J (2020) Dynamics and coherence resonance in a thermosensitive neuron driven by photocurrent. Chin Phys B 29:098704. https://doi.org/10.1088/1674-1056/ab9dee

Yang XL, Yu YH, Sun ZK (2017) Autapse-induced multiple stochastic resonances in a modular neuronal network. Chaos 27:083117. https://doi.org/10.1063/1.4999100

Yang Y, Cui Y, Sang K, Dong Y, Ni Z, Ma S, Hu H (2018) Ketamine blocks bursting in the lateral habenula to rapidly relieve depression. Nature 554(7692):317–322. https://doi.org/10.1038/nature25509

Yang CZ, Liu Z, Wang QY, Luan GM, Zhai F (2021) Epileptic seizures in a heterogeneous excitatory network with short-term plasticity. Cogn Neurodyn 15:43–51. https://doi.org/10.1007/s11571-020-09582-w

Yao CG, He ZW, Nakano T, Qian Y, Shuai JW (2019) Inhibitory-autapse-enhanced signal transmission in neural networks. Nonlinear Dyn 97(2):1425–1437. https://doi.org/10.1007/s11071-019-05060-z

Yilmaz E, Ozer M (2015) Delayed feedback and detection of weak periodic signals in a stochastic Hodgkin–Huxley neuron. Physica A 421:455–462. https://doi.org/10.1016/j.physa.2014.10.096

Yilmaz E, Ozer M, Baysal V, Perc M (2016) Autapse-induced multiple coherence resonance in single neurons and neuronal networks. Sci Rep 6:30914. https://doi.org/10.1038/srep30914

Yilmaz E, Baysal V, Perc M, Ozer M (2016) Enhancement of pacemaker induced stochastic resonance by an autapse in a scale-free neuronal network. Sci China Technol Sci 59:364–370. https://doi.org/10.1007/s11431-015-5984-z

Yin LP, Zheng R, Ke W, He QS, Zhang Y, Li JL, Wang B, Mi Z, Long YS, Rasch MJ, Li TF, Luan GM, Shu YS (2018) Autapses enhance bursting and coincidence detection in neocortical pyramidal cells. Nat Commun 9:4890. https://doi.org/10.1038/s41467-018-07317-4

Zhao ZG, Gu HG (2017) Transitions between classes of neuronal excitability and bifurcations induced by autapse. Sci Rep 7:6760. https://doi.org/10.1038/s41598-017-07051-9

Zhao ZG, Jia B, Gu HG (2016) Bifurcations and enhancement of neuronal firing induced by negative feedback. Nonlinear Dyn 86(10):1549–1560. https://doi.org/10.1007/s11071-016-2976-x

Zhao ZG, Li L, Gu HG (2018) Dynamical mechanism of hyperpolarization-activated non-specific cation current induced resonance and spike-timing precision in a neuronal model. Front Cell Neurosci 12:62. https://doi.org/10.3389/fncel.2018.00062

Zhao ZG, Li L, Gu HG, Gao Y (2020a) Different dynamics of repetitive neural spiking induced by inhibitory and excitatory autapses near subcritical Hopf bifurcation. Nonlinear Dyn 99:1129–1154. https://doi.org/10.1007/s11071-019-05342-6

Zhao ZG, Li L, Gu HG (2020b) Excitatory autapse induces different cases of reduced neuronal firing activities near Hopf bifurcation. Commun Nonlinear Sci Numer Simul 85:105250. https://doi.org/10.1016/j.cnsns.2020.105250